RESEARCH ARTICLE

The copy-number and varied strengths of MELT motifs in Spc105 balance the strength and responsiveness of the spindle assembly checkpoint

Babhrubahan Roy, Simon JY Han†, Adrienne Nicole Fontan‡, Ajit P Joglekar*

Cell and Developmental Biology, University of Michigan Medical School, Ann Arbor, United States

Abstract During mitosis, the Spindle Assembly Checkpoint (SAC) maintains genome stability while also ensuring timely anaphase onset. To maintain genome stability, the SAC must be strong to delay anaphase even if just one chromosome is unattached, but for timely anaphase onset, it must promptly respond to silencing mechanisms. How the SAC meets these potentially antagonistic requirements is unclear. Here we show that the balance between SAC strength and responsiveness is determined by the number of 'MELT' motifs in the kinetochore protein Spc105/KNL1 and their Bub3-Bub1 binding affinities. Many strong MELT motifs per Spc105/KNL1 minimize chromosome missegregation, but too many delay anaphase onset. We demonstrate this by constructing a Spc105 variant that trades SAC responsiveness for much more accurate chromosome segregation. We propose that the necessity of balancing SAC strength and responsiveness drives the dual evolutionary trend of the amplification of MELT motif number, but degeneration of their functionally optimal amino acid sequence.

***For correspondence:** ajitj@umich.edu

Present address: †University of Cincinnati College of Medicine, Cincinnati, United States; ‡Massachusetts Institute of Technology, Cambridge, United States

Competing interests: The authors declare that no competing interests exist.

Funding: See page 21

Received: 12 January 2020
Accepted: 29 May 2020
Published: 01 June 2020

Reviewing editor: Jon Pines, Institute of Cancer Research Research, United Kingdom

Introduction

To achieve accurate chromosome segregation, the dividing cell executes three processes prior to anaphase onset: (1) assembly of a bipolar spindle, (2) capture of unattached chromosomes by the spindle, and (3) bipolar attachment of each chromosome to microtubules emanating from opposite spindle poles. Proper execution and completion of these processes requires some minimum amount of time. Moreover, the time required for chromosome capture and biorientation is not completely predictable; stochastic events can introduce significant delays in their completion. To provide a minimum amount of time to the cell for spindle formation and to prolong cell division as necessary to ensure chromosome attachment to the spindle, the eukaryotic cell uses a signaling mechanism known as the 'Spindle Assembly Checkpoint' (SAC). The SAC is activated by a signaling cascade that operates from the kinetochore, a protein structure that mediates chromosome attachment to the spindle. When unattached, the kinetochore produces an anaphase-inhibitory signal to delay cell division (***Musacchio, 2015***). To ensure both accurate chromosome segregation and timely anaphase onset, the dividing cell must ensure that SAC signaling is strong, but also responsive to silencing mechanisms. Whether such balanced SAC operation is important, and if so, how it is achieved remains poorly understood.

A key determinant of the strength of the SAC is the conserved kinetochore protein Spc105, which provides the physical scaffold for SAC signaling. Spc105 and its homologs possess a large, unstructured phosphodomain containing short sequence repeats commonly referred to as 'MELT' motifs because of their consensus sequence in yeast and humans. Phosphorylation of a MELT motif by the conserved Mps1 kinase turns on the SAC signaling cascade and results in the generation of the

anaphase-inhibitory signal (***London et al., 2012***; ***Meadows et al., 2011***; ***Vleugel et al., 2013***; ***Figure 1A***). Even just one phosphorylated MELT motif can delay anaphase in yeast and human cells (***Aravamudhan et al., 2016***; ***Chen et al., 2019***; ***Krenn et al., 2014***). Therefore, the number of MELT motifs per Spc105 molecule is a crucial determinant of the strength of SAC signaling; many MELT motifs per Spc105 are expected to endow it, and by extension the kinetochore, with a correspondingly larger signaling capacity. Indeed, Spc105 and its homologs typically contain many MELT motifs, for example six in budding yeast and nineteen in humans (***Tromer et al., 2015***), and the large MELT motif number is thought to be essential for implementing a strong SAC (***Chen et al., 2019***; ***Krenn et al., 2014***; ***Vleugel et al., 2015***; ***Vleugel et al., 2013***; ***Zhang et al., 2014***). However, when budding yeast and human cells are treated with high doses of the microtubule poison nocodazole, only a small fraction of the MELT motifs,~20 and~35% respectively, engage in SAC signaling, and even fewer MELT motifs are sufficient for arresting cell division (***Aravamudhan et al., 2016***; ***Vleugel et al., 2015***; ***Vleugel et al., 2013***; ***Zhang et al., 2014***). These observations bring into

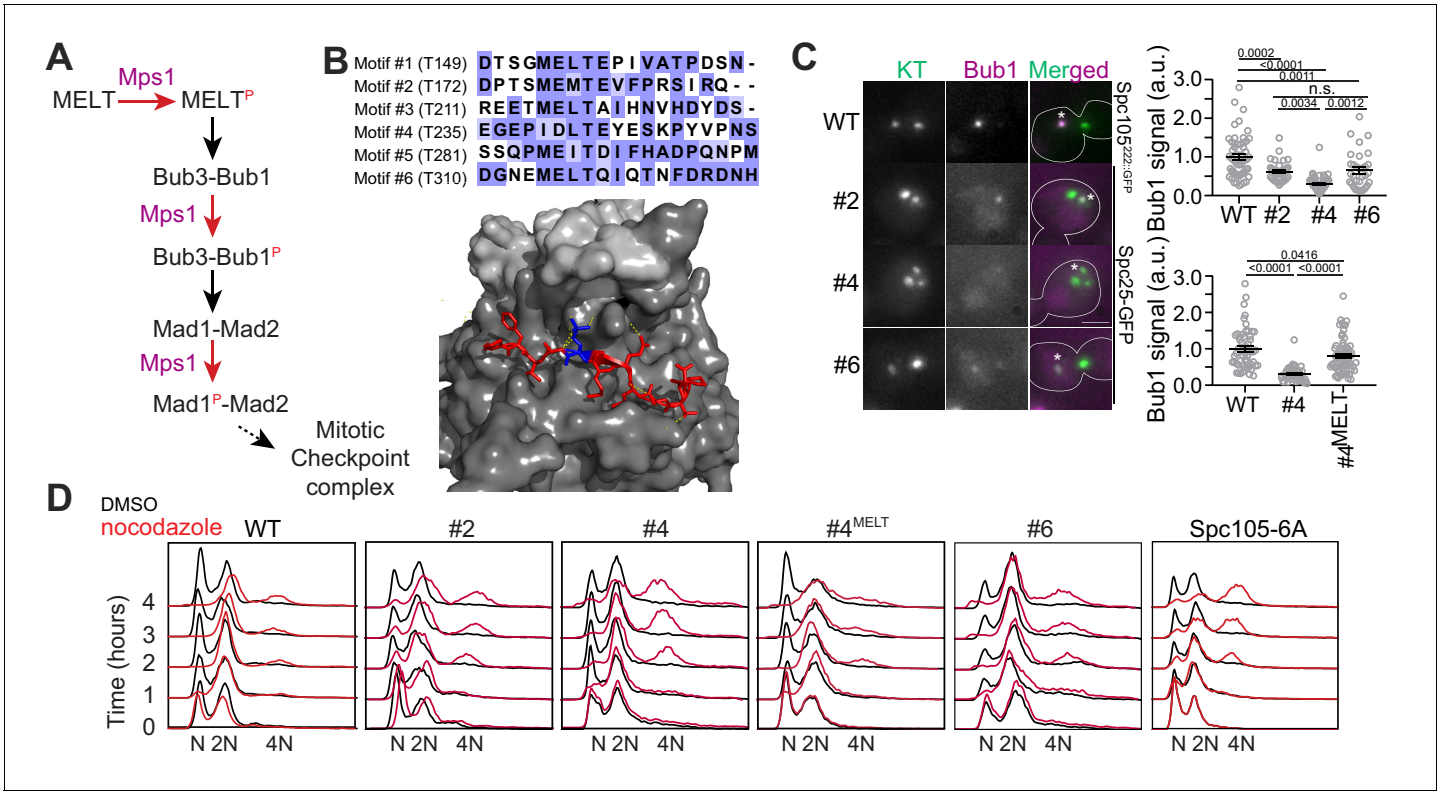

Figure 1. Only one MELT motif per Spc105 is sufficient for SAC signaling in nocodazole-treated cells. (**A**) A simplified schematic of the signaling cascade of the SAC in budding yeast (Mad3/BubR1, Cdc20, etc. are not shown). (**B**) Top: amino acid sequence alignment for the six MELT motifs in the *Saccharomyces cerevisiae* Spc105. Bottom: Crystal structure of the MELpT-Bub3-Bub1 complex (adapted from PDB 4BL0 and 2I3S). Note that the phosphothreonine (shown in blue, inter-chain hydrogen bonds highlighted by dashed lines) buried in a grove on Bub3 surface. (**C**) Micrographs display representative images of nocodazole-treated yeast cells with fluorescently labeled kinetochores and Bub1-mCherry. Asterisks mark Bub1-mCherry colocalized with the unattached kinetochore clusters. Kinetochores in the other, larger cluster proximal to the spindle pole bodies do not recruit SAC proteins, presumably because they remain attached to short microtubule stubs at the spindle pole bodies. Scale bar ~3.2 μm. Scatterplots show the quantification of Bub1-mCherry fluorescence in wild-type (WT) and mutant strains (labeled by the number designation of the active MELT motif). Fluorescence values have been normalized to the average Bub1-mCherry fluorescence in wild-type cells. (mean+ s.e.m. Top: n = 55, 33, 51 and 32 for WT, #2, #4 and #6 respectively, accumulated from two technical replicates. Bottom: n = 55, 92 and 68 for WT, #2 and #6 respectively, pooled from two technical replicates. n.s. Not significant. (**D**) Quantification of DNA content in cells treated with nocodazole using flow cytometry. The assay was performed once.

The online version of this article includes the following source data and figure supplement(s) for figure 1:

Source data 1. The data for two scattered plots shown in ***Figure 1C***, right top and bottom.
Figure supplement 1. A The fraction of cells with 4N ploidy in the flow cytometry experiments shown in ***Figure 1D***.
Figure supplement 1—source data 1. Data required to prepare the graph shown in ***Figure 1—figure supplement 1A***.

question the simple model that the large number of MELT motifs achieve a correspondingly large amplification of the signaling capacity of Spc105.

The amino acid sequence of a MELT motif directly determines its SAC signaling activity, because these residues directly bind to the Bub3-Bub1 complex (***Figure 1B***; ***Primorac et al., 2013***). However, bioinformatics analyses show that in many eukaryotes, the MELT motif number as well as sequence is evolving rapidly due to: (a) duplication and loss of existing MELT motifs, and (b) sequence divergence of some of the MELT motifs from the consensus amino acid sequence (***Tromer et al., 2015***). In human and yeast cells, sequence divergence has created many MELT motifs with a weak ability to bind Bub3-Bub1, and hence a significantly lower signaling activity (***Primorac et al., 2013***; ***Vleugel et al., 2015***; ***Vleugel et al., 2013***). Why Spc105 contains a large number of MELT motifs, but then uses only a small fraction under certain experimental conditions, and why the sequence of many MELT motifs has diverged from the functionally optimal sequence remains unknown. Here, we show that the number of MELT motifs in Spc105 and their sequences strongly influence the strength of SAC signaling and its responsiveness to silencing mechanisms.

Results

In nocodazole-treated budding yeast cells, Spc105 with just one MELT motif is sufficient to effect a prolonged mitotic arrest

Three of the six motifs in the budding yeast Spc105 possess the consensus amino acid sequence ('MELT'), and these are likely to display higher Bub3-Bub1 binding affinity than the other three motifs possessing divergent amino acid sequences (***London et al., 2012***). We wanted to verify this expectation and also determine the minimum number of MELT motifs per Spc105 required to maintain a prolonged mitotic block.

We created three different yeast strains each expressing a Spc105 mutant wherein either motif #2, #4, or #6 is the only phosphorylatable, active motif (numbering follows ***Figure 1B***). To study SAC signaling in these strains, we destroyed the mitotic spindle using the microtubule poison nocodazole to activate the SAC. To measure the signaling activity of each motif, we quantified the recruitment of Bub1-mCherry by unattached kinetochore clusters in nocodazole-treated cells (***Figure 1C***, Materials and methods). To assess the SAC strength in these strains, we quantified the ploidy of cell populations over four hours of nocodazole treatment (***Figure 1D***). After 4 hr of nocodazole treatment, the wild-type population maintained 2N ploidy. However, a small fraction of cells slipped out of the SAC arrest to attain 4N ploidy (***Figure 1D***, left). In contrast, in the SAC-deficient *spc106-6A* strain, wherein all six MELT motifs are non-phosphorylatable, the majority of the cells attained 4N ploidy after 4 hr (***Figure 1D***, rightmost, the percentage of cells with 4N ploidy for all strains is tabulated in ***Supplementary file 1***. Also see ***Figure 1—figure supplement 1***). Motif #2 and #6 supported robust SAC signaling as judged by the ability of the mutant cells to maintain 2N ploidy over the 4 hr long duration of the nocodazole-induced mitotic arrest despite recruiting ~50% less Bub1 compared to wild-type Spc105 (the leftmost graph in ***Figure 1D***, the small fraction of 4N ploidy cells emerging after >2 hr of nocodazole treatment represents cells that slipped out of the SAC arrest). Motif #4 recruited significantly less Bub1-mCherry than the other two, which is consistent with its weaker affinity for binding recombinant Bub3-Bub1 complex in vitro (***Overlack et al., 2015***). It also resulted in a weaker SAC as evidenced by the emergence of a considerable fraction of tetraploid cells 3–4 hr post treatment. Replacement of the divergent amino acid sequence of this motif ('IDLT') with the consensus sequence ('MELT') improved both Bub1 recruitment and SAC strength. Thus, the amino acid sequence of each MELT motif primarily determines its ability to recruit Bub3-Bub1 and its contribution to SAC signaling (***Figure 1C–D***). Furthermore, just one strong MELT motif per Spc105 is sufficient to induce a prolonged mitotic arrest upon spindle depolymerization by nocodazole.

Multiple MELT motifs per Spc105 are essential when chromosome attachment to the spindle and biorientation is challenged

Quantification of SAC strength in nocodazole-treated cells has a significant drawback: it measures SAC strength in the presence of a large and unchanging number of unattached kinetochores. Due to the continued presence of nocodazole in growth media, spindle assembly does not

occur and as a result most, if not all, kinetochores remain unattached. Consequently, even when the signaling capacity of individual kinetochores is impaired, the cumulative output of many signaling kinetochores may still impose a prolonged mitotic arrest under the steady state signaling condition (in regard to the number of unattached kinetochores). This situation occurs rarely, if ever, during the course of a normal cell division. As chromosomes attach to the newly formed spindle, the number of unattached kinetochores decreases rapidly until only a few or just one kinetochore remains unattached. In this dynamic situation, the SAC must reliably delay anaphase irrespective of the number of unattached kinetochores. Therefore, we explored the effect of individual MELT motifs on SAC performance in cells containing small numbers of unattached kinetochores.

We first established the conditions necessary to create small numbers of unattached kinetochores using low doses of the microtubule-destabilizing drug benomyl. Unlike nocodazole treatment, which destroys the spindle, benomyl at low concentrations increases microtubule dynamicity and therefore challenges spindle formation and chromosome biorientation. Wild-type cells still grow under this condition, but any genetic defects in SAC signaling or chromosome biorientation can cause poor growth or inviability (***Hoyt et al., 1991***). We hypothesized that cells grown in the presence of benomyl will more frequently contain small numbers of unattached kinetochore, and therefore require a strong SAC for proliferation. To test this, we followed chromosome biorientation by marking the centromere of chromosome IV with a TetO array (***Figure 2A*** left). In normal media, yeast cells released from a G1 arrest bioriented chromosome IV in ~45 min and completed anaphase by 75 min. In media containing low doses of benomyl, both events were significantly delayed. In most cells, chromosome IV did not achieve biorientation even after 105 min post release (the duration of the experiment was limited to 105 min, because cells not affected by the treatment entered the next cell cycle after this point, which complicated the analysis). In a small fraction of the cells, chromosome IV was displaced from the spindle and was likely unattached. To assess the attachment state of all the chromosomes under the same conditions, we imaged yeast cells expressing $Spc105^{222::GFP}$ (GFP inserted after the 222^{nd} residue in Spc105) and Bub1-mCherry. Most cells contained a significantly smaller number of unattached kinetochores recruiting Bub1-mCherry. Importantly, the number of unattached kinetochores per cell was significantly smaller when compared to the average number of unattached kinetochores per cell after nocodazole treatment (5 +/- 4 per cell versus to ~10 in nocodazole-treated cells (***Aravamudhan et al., 2016***; ***Figure 2A*** right). Cells with unattached kinetochores persisted 105 min after the introduction of benomyl (***Figure 2A*** right).

We next examined the effects of benomyl on a strain expressing a mutant Spc105 with only two phosphorylatable motifs: #2 and #6, to test whether the SAC might be weaker under this condition. Each of the two MELT motifs by itself supports robust SAC signaling in nocodazole-treated cells (***Figure 1D***). However, 75 min after release from the G1 arrest into media containing benomyl more mutant cells were in anaphase compared to wild-type cells, as evidenced by elongated spindles and sister kinetochores segregated in the mother and bud (***Figure 2B***). It should be noted that most cells are expected to contain unattached kinetochores at this time point. Therefore, these observations together imply that many cells expressing Spc105 with motif #2 and #6 are unable to prevent anaphase onset even though they contain small numbers of unattached kinetochores. Accordingly, many cells expressing the mutant Spc105 displayed elongated spindles with lagging/unaligned kinetochores (***Figure 2—figure supplement 1A***).

If cells expressing a Spc105 mutant mis-segregate their chromosomes more frequently than wild-type cells as a result of weak SAC signaling, apopulation of these cells should display more frequent cell death, and hence reduced growth rates. To test this, we quantified the growth of yeast strains expressing Spc105 mutants carrying different combinations of MELT motifs in normal media and media containing benomyl by quantifying absorbance at 600 nm wavelength (OD_{600}, ***Figure 2C***). In normal media, the mutant strains showed relatively minor differences in their growth rate and the peak cell density (due to nutrient depletion) compared to the wild-type strain (***Figure 2C***, top left). However, stark differences in growth rate and maximal cell density were apparent in media containing benomyl (***Figure 2C***, top right; for reference a schematic of the MELT motif position and sequences is also included at the bottom of ***Figure 2C*** and in ***Figure 2—figure supplement 1B***). Strains expressing Spc105 mutants with either motif #2 alone or motif #2 and #6 together grew at slower rates and reached significantly lower cell densities than the wild-type strain. Spc105 mutants containing either the first two or three MELT motifs (two of which possess the consensus amino acid sequence, and hence are expected to be strong), supported nearly normal growth in benomyl-

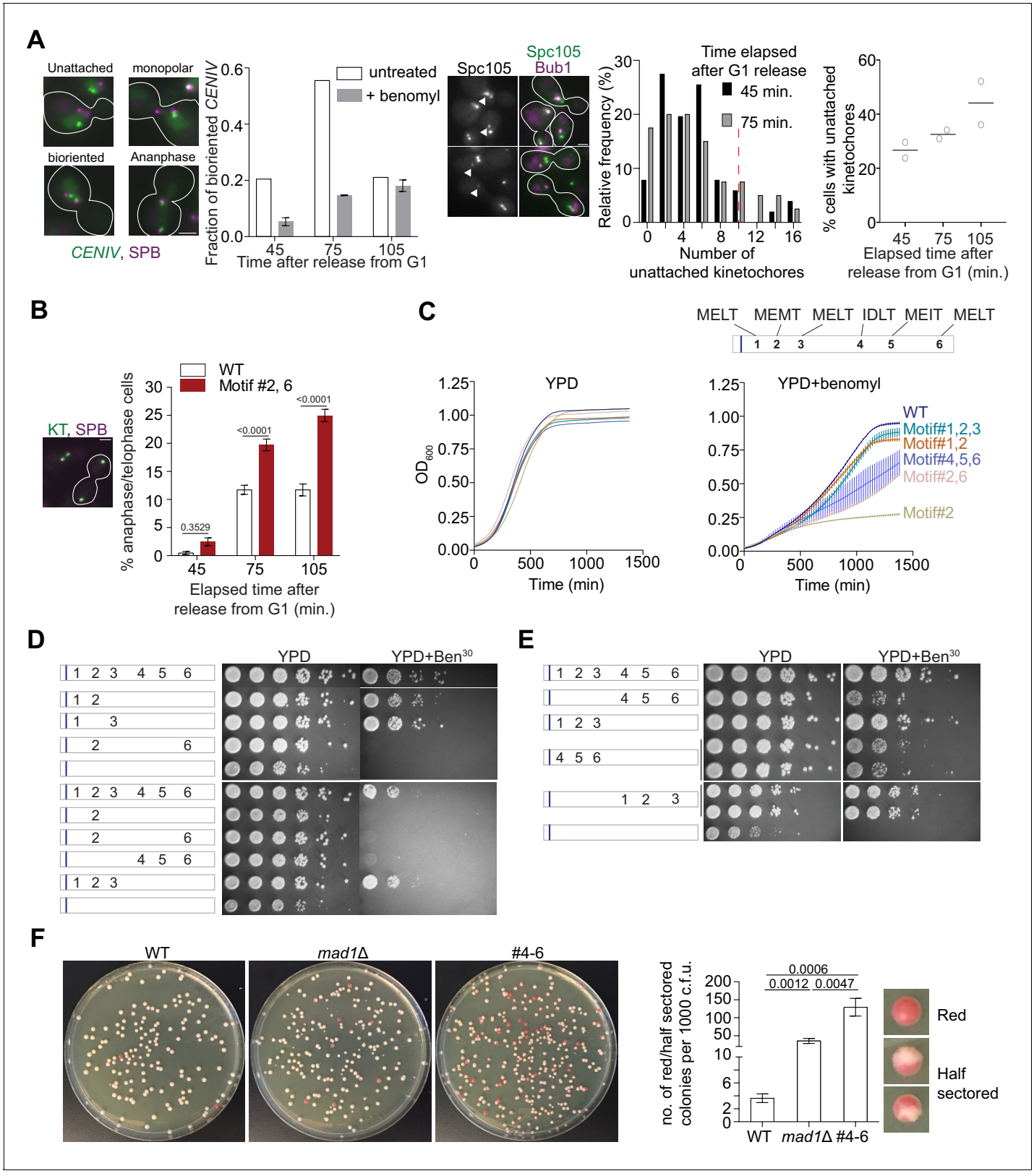

Figure 2. More than one high affinity MELT motifs are necessary to minimize chromosome loss. (**A**) Effects of benomyl on chromosome biorientation. Left: Kinetics of chromosome IV biorientation visualized using a centromere-proximal TetO array. Micrographs depict representative images of cells showing fluorescently labeled TetR-GFP bound to the TetO array and Spindle Pole Bodies (SPB). Scale bar ~3.2 μm. Second from the left: Quantification of the fraction of cells with bioriented chromosome IV. Note that the reduced fraction of untreated cells with bioriented chromosomes

Figure 2 continued on next page

Figure 2 continued

105 min after release from G1 is because most cells complete anaphase by this time. (n = 259, 252 and 398 at 45, 75 and 105 min respectively in normal media, one repeat. n = 855, 816 and 626 respectively at 45, 75 and 105 min in benomyl-containing media from three technical repeats). When the two *CENIV* foci were unresolvable and localized in the vicinity of one of the two SPBs, they were scored as monopolar attachments. When the two *CENIV* foci were clearly separated from each other and located along the spindle axies, they were considered to be bioriented. Middle: Representative micrographs of cells grown in benomyl media containing unattached kinetochores recruiting Bub1. Arrow heads indicate the unattached kinetochores with Bub1 localizations. Scale bar ~3.2 μm. Right: Quantification of the number and frequency distribution of unattached kinetochores in yeast cells growing in media containing benomyl. The unattached kinetochore number was estimated by comparing the Spc105-GFP fluorescence from the unattached kinetochore cluster (marked by Bub1-mCherry recruitment) with the total fluorescence from the kinetochores along the spindle axis. (n = 686, 501 and 543 at 45, 75 and 105 min respectively, pooled from two technical repeats). Red dashed line in relative frequency plot indicates the average number of unattached kinetochores observed after 90 min nocodazole treatment of wild type yeast cell (***Aravamudhan et al., 2016***). (**B**) Left: Micrograph displays representative cells in metaphase and anaphase in benomyl-containing media. Scale bar ~3.2 μm. Right: Quantification of the number of anaphase cells observed after the indicated time following release from a G1 arrest for the indicated strains. (mean+ s.e.m, n = 1029, 889 and 992 at 45, 75 and 105 min respectively for WT cells, pooled from three experimental repeats. n = 890, 864 and 812 at 45, 75 and 105 min time points respectively for #2,6, pooled from three technical replicates). (**C**) Top: Schematic of the Spc105 phosphodomain with the amino acid sequence indicated at the top. Bottom: Quantification of the evolution of cell density of the indicated strains in rich media (left) and media-containing benomyl (right). (**D–E**) Assessment of the sensitivity of yeast strains to benomyl using the spotting assay. Schematics on the left show the active motif number and its position. The blue bar represents the 'basic patch' in Spc105, which promotes PP1 recruitment. The photographs on the right show the results of spotting a serial dilution of yeast cells on rich media (YPD) and media containing benomyl (20 or 30 μg/ml). (**F**) Assessment of chromosome loss by colony sectoring assay. Left: Images of WT, *mad1*Δ and #4–6 colonies grown in YPD plates. Right: Bar graph shows the rate of loss of *SUP11* containing chromosome fragment measured as the number of red/half red colonies (example shown on the right) for every 1000 colonies plated. N = 5081, 4406 and 4965 for WT, *mad1*Δ and #4–6 respectively, pooled from at least six technical repeats.

The online version of this article includes the following source data and figure supplement(s) for figure 2:

Source data 1. Data for graphs depicted in ***Figure 2A, B, C and F***.

Figure supplement 1. Requirements of the MELT motif number per Spc105 and their affinity for survival on media containing benomyl.

Figure supplement 1—source data 1. Data required for the graph shown in ***Figure 2—figure supplement 1A***.

Figure supplement 2. Multiple, strong MELT motifs per Spc105 are essential for cell survival when chromosome biorientation is challenged by conditionally disrupting the mitotic Cik1 functions.

Figure supplement 2—source data 1. Data needed for the plots shown in ***Figure 2—figure supplement 2B*** top right and 2B bottom right.

Figure supplement 3. The difference in the SAC signaling activities of the first three and last three MELT motifs in Spc105 is detectable in benomyl-containing media, but not in cells treated with nocodazole.

Figure supplement 3—source data 1. Data required in the graphs mentioned in ***Figure 2—figure supplement 3A*** top, C right top, C right bottom, D right top and D right bottom.

containing media. Interestingly, the Spc105 mutant with only the last three MELT motifs active grew more slowly and reached lower maximal cell density. Both results are indicative of a weaker SAC. They suggest that in cells containing a small number of unattached kinetochores at least two, strong MELT motifs are necessary for cell survival, and the presence of all six MELT motifs in Spc105 ensures maximal population growth. We confirmed these quantitative findings by spotting serial dilutions of yeast cultures on benomyl media (***Figure 2D***).

The positions of MELT motifs, their role in Sgo1 recruitment, or pleiotropic effects of benomyl do not explain the correlations between MELT motif mutations and benomyl sensitivity

The observed pattern of benomyl sensitivity of the Spc105 mutants may arise due to reasons that are not directly related to the amino acid sequence of the MELT motifs. One possible reason is that the MELT motifs located distally in the Spc105 phosphodomain are situated further away from Mps1 bound to the CH-domains of the Ndc80 complex, and they are therefore less efficiently phosphorylated as compared to the anteriorly located MELT motifs (***Aravamudhan et al., 2015***; ***Hiruma et al., 2015***; ***Ji et al., 2015***; ***Kemmler et al., 2009***). However, even when we swapped the positions of the first three and last three MELT motifs, this did not change the benomyl sensitivities of the two strains (***Figure 2E***). The lack of correlation persisted even in Spc105 mutants containing only one phosphorylatable MELT motif (see ***Figure 2—figure supplement 1C–D***). Thus, the amino acid sequence, and not the position of MELT motifs in the phosphodomain, is the sole determinant of their SAC signaling activity.

The differential recruitment of the centromeric protein Sgo1, a factor that is crucial for chromosome biorientation and error correction, can also explain in differential benomyl sensitivities of the Spc105 mutants (**Kawashima et al., 2010**). Because Bub1 kinase activity promotes the centromeric recruitment of Sgo1, reduced Bub1 recruitment by the Spc105 mutants will reduce centromeric Sgo1, and reduced Sgo1 recruitment will result in increased chromosome missegregation independently of SAC signaling. However, the differences in the benomyl sensitivity between two strains expressing *spc105* mutants containing only strong (#1–3) or weak (#4–6) MELT motifs persisted, even when Sgo1 recruitment to the centromere was either decoupled from Bub1 recruitment (*bub1*$^{\Delta kinase}$; **Figure 2—figure supplement 1E**) or completely abolished (*sgo1*Δ; Fig **Figure 2—figure supplement 1F**). Thus, reduced Sgo1 recruitment by the Spc105 mutants does not fully explain the observed differences in their benomyl-sensitivity.

It should be noted that the strains expressing Spc105 variants with just one active MELT motif as well as the *sgo1*Δ and *bub1*$^{\Delta kinase}$ mutants cannot grow on benomyl. Therefore, to make these benomyl-sensitivity studies possible, we mutated the anterior basic patch in Spc105 (101-RRRK-104:: AAAA). This mutation reduces PP1 binding to Spc105, and minimizes the inadvertent stabilization of syntelic attachments by PP1 (**Roy et al., 2019**). Consequently, chromosome biorientation is significantly improved in these strains, which enables them to grow in benomyl containing media (**Roy et al., 2019**).

Finally, benomyl affects microtubule dynamics throughout the cell cycle creating the possibility that reasons unrelated to SAC strength contribute to the benomyl sensitivity of the mutant strains. To verify that the observed differences among the mutant strains were mainly due to a weaker SAC, we disrupted the mitotic functions of the kinesin Kar3 in strains expressing Spc105 mutants with either strong or weak MELT motifs (**Jin et al., 2012**). This disruption impedes chromosome capture by spindle microtubules and also delays bipolar spindle formation (**Jin et al., 2012**; **Tanaka et al., 2005**). Consequently, a robust SAC becomes essential for maintaining genome stability. We observed the same correlations between the strength of active MELT motifs in Spc105 mutants and cell viability in this assay as the benomyl sensitivity experiments (**Figure 2—figure supplement 2A** and **Figure 2—figure supplement 2B**). Therefore, we conclude that differences in the sensitivity of Spc105 mutant strains mainly arise from differences in their SAC signaling strengths.

Spc105 mutants containing only weak MELT motifs experience high rates of chromosome missegregation during unperturbed cell division

All the experiments so far examined changes in the SAC signaling strength of Spc105 mutants under stressful conditions. To reveal whether the impaired SAC signaling activity mediated only by the weak MELT motifs in Spc105 translates into chromosome missegregation under normal conditions, we used the colony sectoring assay (**Duffy and Hieter, 2018**; **Hieter et al., 1985**). In this assay, chromosome missegregation frequency is quantified for an artificial, linear yeast chromosome. Yeast cells that inherit this chromosome form white colonies, but those that lose the artificial chromosome due to missegregation form colonies that are red/pink in color. Therefore, the frequency of the white to red/pink color transformation provides a quantitative read-out of chromosome missegregation events.

We studied the impact of the weak SAC signaling activity displayed by Spc105$^{\#4\text{-}6}$ (mutant containing motifs #4–6 as the phosphorylatable motifs) under normal growth conditions using the colony color assay. We found that chromosome missegregation events were significantly more frequent in cells expressing Spc105$^{\#4\text{-}6}$ compared a wild-type strain (we scored both half-sectored and fully red colonies as chromosome mis-segregation events; see Materials and methods for details). In fact, they were more frequent even when compared to the *mad1*Δ strain lacking a functional SAC (**Figure 2F**). It is important to note that SAC signaling in this mutant strain is indistinguishable from the SAC signaling in a wild-type strain in the traditional assay using nocodazole treatment, (see Bub3-mCherry recruitment and flow cytometry data in **Figure 2—figure supplement 3A**). The weaker SAC signaling in this strain is observed only when the SAC is activated by a small number of unattached kinetochores (**Figure 2—figure supplement 3B**). Surprisingly, the frequency of chromosome missegregation in cells expressing Spc105$^{\#4\text{-}6}$ is significantly higher even than the SAC null-strain. The most likely explanation for the higher missegregation frequency in this mutant is that the kinetochores in prometaphase recruit lower amounts of Bub3-Bub1, and therefore, lower amounts

of Sgo1 (*Figure 2—figure supplement 3C–D*). The lower Sgo1 recruitment ultimately impairs chromosome biorientation, and thus further elevates chromosome missegregation frequency.

These results demonstrate that Spc105 containing more than one, strong MELT motif is essential to ensure accurate chromosome segregation during normal cell division. They also suggest that in cells containing a large and unchanging number of unattached kinetochores, defects in the signaling output of individual kinetochores (e.g. due to Spc105 containing weak MELT motifs) can be masked by the cumulative signaling output of many, simultaneously signaling kinetochores.

The requirement of many, strong MELT motifs per Spc105 for accurate chromosome segregation raises a critical question: why wasn't the functionally optimal amino acid sequence retained by all six MELT motifs in Spc105? The likely explanation is that many high affinity MELT motifs reduce the responsiveness of the SAC to silencing mechanisms. In budding yeast, the SAC is silenced when the SAC signaling proteins unbind from the kinetochore, and they are prevented from rebinding by PP1-mediated dephosphorylation. An intriguing hypothesis is that the high affinity MELT motifs are resistant to dephosphorylation, and hence they retard SAC silencing. The structure of the MELpT-Bub3-Bub1$^{289\text{-}359}$ complex shows that the phosphorylated threonine residue is lodged in a positively charged groove on Bub3 surface (*Primorac et al., 2013*). This mode of binding implies that the Bub3-Bub1 complex will sterically interfere with PP1 by shielding the phosphothreonine in the MELT motif (see *Figure 1B*). Consequently, the rate of dephosphorylation of a MELT motif may be inversely correlated with its Bub3-Bub1 binding affinity, and by extension, its amino acid sequence. Given that only two strong MELT motifs are sufficient for a strong SAC, sequence divergence of some of the MELT motifs may be desirable, because this allows the mutants to trade SAC strength for responsiveness, achieving timely anaphase onset and hence a rapid growth.

Kinetochore-microtubule attachment reduces Mps1 kinase activity in the kinetochore, priming the SAC for silencing

Before investigating the role that the MELT motif sequence may play in determining SAC responsiveness to silencing, we found it necessary to fully understand the mechanisms of SAC silencing itself. In budding yeast, two mechanisms contribute to SAC silencing: (1) the physical separation of the Spc105 phosphodomain from Mps1 kinase bound to the Calponin-Homology domains of the Ndc80 complex (*Aravamudhan et al., 2015*), and (2) recruitment of the Protein Phosphatase I (PP1) via the conserved 'RVSF' motif in N-terminus of Spc105 to dephosphorylate the MELT motifs and disrupt the recruitment of SAC proteins (*Liu et al., 2010*; *London et al., 2012*; *Meadows et al., 2011*; *Rosenberg et al., 2011*). We wanted to determine why both mechanisms are necessary for anaphase onset, and how their contributions affect the responsiveness of the SAC to silencing.

In budding yeast, Mps1 kinase binds to the CH-domains of Ndc80 even after end-on attachments form (*Aravamudhan et al., 2015*; *Koch et al., 2019*). This implies that a gradient of Mps1 kinase activity is likely to exist in bioriented yeast kinetochores. Although the N-terminus of Spc105 is on average ~30 nm away from the CH-domains (*Figure 3—figure supplement 1A*), we wanted to ascertain whether the MELT motifs may extend past this average position to interact with Mps1 bound to the CH-domains. To ascertain this, we measured FRET between a donor fluorophore (GFP) placed at five different locations along Spc105, and an acceptor (mCherry) placed at two positions in the kinetochore that demarcate the region expected to contain the Spc105 phosphodomain (see cartoon in *Figure 3—figure supplement 1A*). We detected weak FRET between Spc105$^{222:GFP}$ (GFP inserted after amino acid 222 in Spc105) and Dad4-mCherry (a subunit of the Dam1 complex, *Figure 3—figure supplement 1A*). This result suggest that Spc105 phosphodomain can extend past its average position toward the high Mps1 kinase activity region of the kinetochore (*Aravamudhan et al., 2014*; *Joglekar et al., 2009*).

The persistence of Mps1 in bioriented kinetochores and the unstructured nature of Spc105 led us to hypothesize that MELT motifs will continue to be phosphorylated even after biorientation, and this may delay SAC silencing. To test this, we tethered an additional Spc105 phosphodomain at different distances from the CH-domains using rapamycin-induced dimerization of Fkbp12 and Frb in asynchronously growing cells (*Figure 3A*). Consistent with our hypothesis, even though the phosphodomain did not activate the SAC when tethered distally from the CH-domains (e.g. at the C terminus of Ndc80), it was robustly phosphorylated as evidenced by the recruitment of Bub3-mCherry (*Figure 3A and B*, also see *Figure 3—figure supplement 1B*). Bub3-mCherry recruitment decreased progressively as the average separation between the tethering point and the CH-domains increased

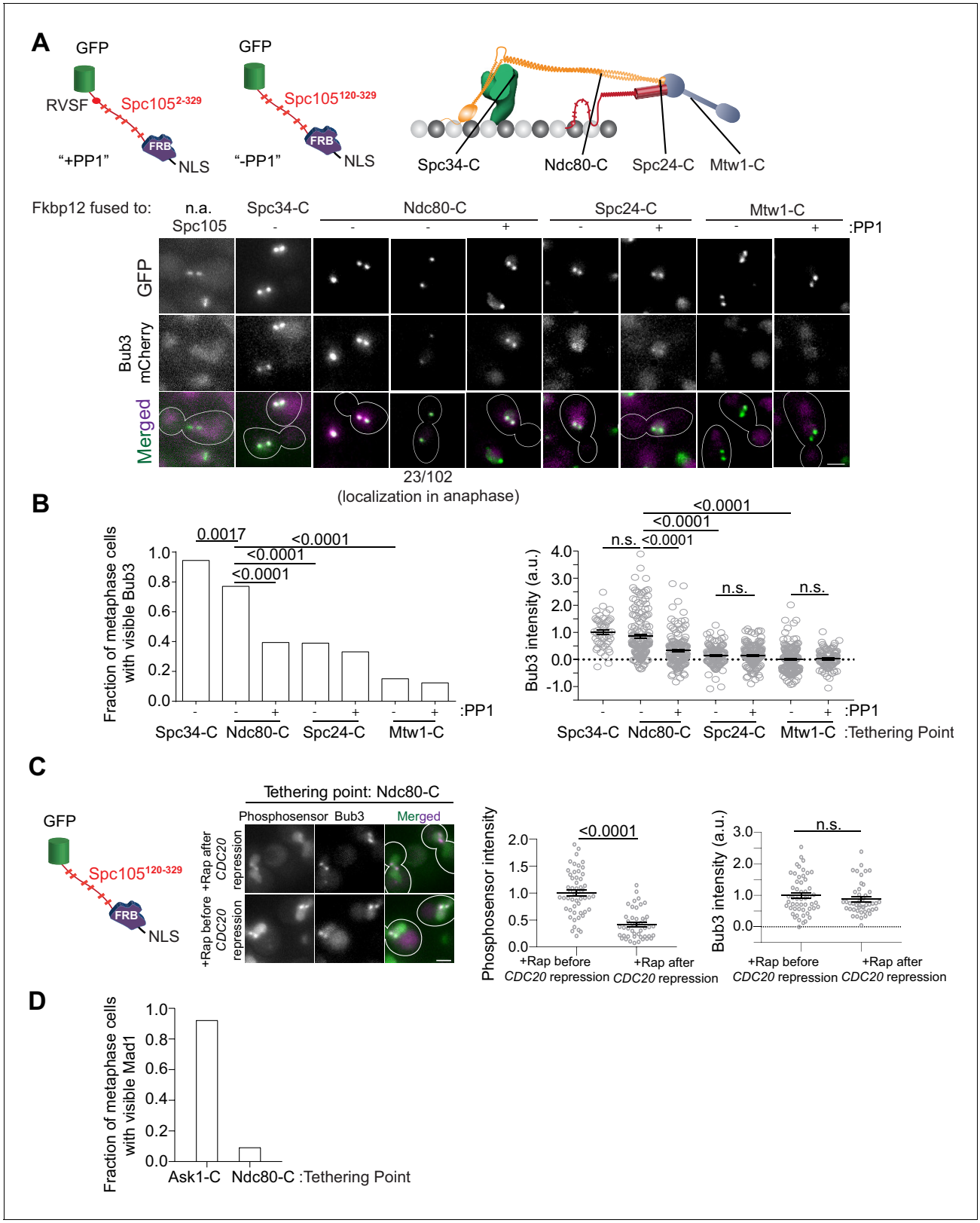

Figure 3. A gradient of Mps1 kinase activity continues to phosphorylate MELT motifs after chromosome biorientation. (**A**) Top left: Cartoons show schematics of the two Spc105 phosphodomains tethered to kinetochore subunits using the rapamycin-induced dimerization of Fkbp12 and Frb domains. Top right: The kinetochore subunits (Spc34-C, Ndc80-C, Spc24-C and Mtw1-C) at which, the phosphodomains were tethered by rapamycin induced dimerization. Bottom: Micrographs show representative images of cycling cells wherein the phosphodomain is tethered to the C-terminus of

Figure 3 continued on next page

Figure 3 continued

the indicated kinetochore subunit. (n.a. - Not Applicable). (**B**) Left: The bar plot shows the scoring of cells with bioriented kinetochore clusters based on whether or not they visibly recruit Bub3-mCherry. (n = 71 for Spc34-C, 109 and 94 for Ndc80-C, 95 and 103 for Spc24-C, 106 and 122 for Mtw1-C, accumulated from two experimental and biological repeats (whenever possible). Right: The scatter plot on the right shows the quantification of Bub3-mCherry fluorescence from all cells with bioriented kinetochore clusters. (mean+ s.e.m. n = 47 for Spc34-C, 159 and 153 for Ndc80-C, 114 and 154 for Spc24-C, 173 and 104 for Mtw1-C, accumulated from two experimental and biological repeats wherever possible). n.s. Not significant. (**C**) Micrographs show the recruitment of Bub3-mCherry by the phosphosensor tethered at the Ndc80 C-terminus in cycling (before *CDC20 repression)* and metaphase arrested cells (after *CDC20* repression). Scatterplots show the relative fluorescence signal from the GFP-tagged phosphosensor and Bub3-mCherry respectively. (mean+ s.e.m. n = 52 and 45 for rapamycin treated samples before and after Cdc20 depletion from two technical replicates). n.s. Not significant. (**D**) Bar graph shows fraction of cells visibly recruiting Mad1-mCherry as shown in the micrographs (n = 242 and 142 for Ask1-C and Ndc80-C respectively).

The online version of this article includes the following source data and figure supplement(s) for figure 3:

Source data 1. Data that are included in the plots of ***Figure 3B*** left and right, 3C left and right and 3D are shown here.

Figure supplement 1. The distribution of the Spc105 phosphodomain in bioriented kinetochores and the position-dependent effects of tethering an additional phosphodomain within the kinetochore.

Figure supplement 1—source data 1. Data required to prepare the plots included in ***Figure 3—figure supplement 1A*** bottom left and right, C and D.

(as measured in bioriented kinetochores, ***Joglekar et al., 2009***). The inclusion of the PP1 recruitment motif in Spc105 (+PP1) reduced, but did not eliminate, Bub3 recruitment (+PP1 in ***Figure 3A***, ***Figure 3—figure supplement 1C***). In fact, a sizeable fraction (~20%) of anaphase cells displayed Bub3-mCherry colocalized with kinetochores. Finally, the phosphodomain recruited Bub3-mCherry even when we tethered it after kinetochore biorientation in metaphase arrested cells indicating that not all of the Bub3 was recruited prior to biorientation (***Figure 3C***). Importantly, we found that the phosphodomain did not recruit Mad1 when it was tethered to a position distal to the CH-domains (***Figure 3D***).

These experiments show that a diminishing gradient of Mps1 kinase activity extends from the CH-domains toward the centromere in bioriented yeast kinetochores, and this residual Mps1 kinase activity likely continues to phosphorylate the MELT motifs. The absence of Mad1 recruitment in these experiments suggests that the residual Mps1 activity is not sufficient to phosphorylate Bub1. It is also possible that PP1 recruitment via Spc105 under prevents Mad1 recruitment. In conclusion, the reduction of Mps1 activity after microtubule attachment primes the SAC for silencing. However, but this is not sufficient to induce anaphase onset; PP1 ensures timely anaphase onset.

PP1-mediated dephosphorylation of Bub1 contributes to SAC silencing, but this silencing mechanism is not as efficient as PP1-mediated dephosphorylation of MELT motifs

PP1 can disrupt the SAC signaling cascade by dephosphorylating several Mps1 targets in recruitment step of the SAC signaling (***Faesen et al., 2017***; ***Ji et al., 2017***; ***London and Biggins, 2014***; ***Tipton et al., 2013***; ***Figure 4A***). This was confirmed by the examination the recruitment of SAC proteins in strains expressing *spc105^{RASA}*, wherein Spc105 cannot recruit PP1 (***Rosenberg et al., 2011***). Bioriented kinetochores in this strain recruited both Bub3 and Mad1 (***Figure 4B***, note that the *spc105^{RASA}* mutation results in lethality unless the SAC is inactivated). In contrast, the tethered phosphodomain recruited Bub1, but not Mad1 (***Figure 3D***). These observations suggested to us that the dephosphorylation of Bub1 by PP1 may suppress Mad1 recruitment to the kinetochore, and thereby silence the SAC.

To test this notion, we created a Bub1 mutant wherein two phosphosites implicated in Mad1 recruitment are replaced with non-phosphorylatable alanine residues, and asked if this mutant rescues the viability of *spc105^{RASA}* strain (***Ji et al., 2017***; ***London and Biggins, 2014***; ***Qian et al., 2017***). The *spc105^{RASA} bub1$^{453A,\ 455A}$* double mutant was viable, indicating that the dephosphorylation of Bub1 by PP1 aids SAC silencing (***Figure 4C***, plate photographs). Surprisingly, however, the SAC was still active in this double mutant as judged by the ability of this strain to maintain 2N ploidy upon a prolonged nocodazole treatment (***Figure 4C***, 2nd plot from the left) and to grow in benomyl-containing media (***Figure 3—figure supplement 1D***). Consistently, Mad1 recruitment to unattached kinetochores in nocodazole-treated cells was diminished, but not eliminated (***Figure 4C***, scatter

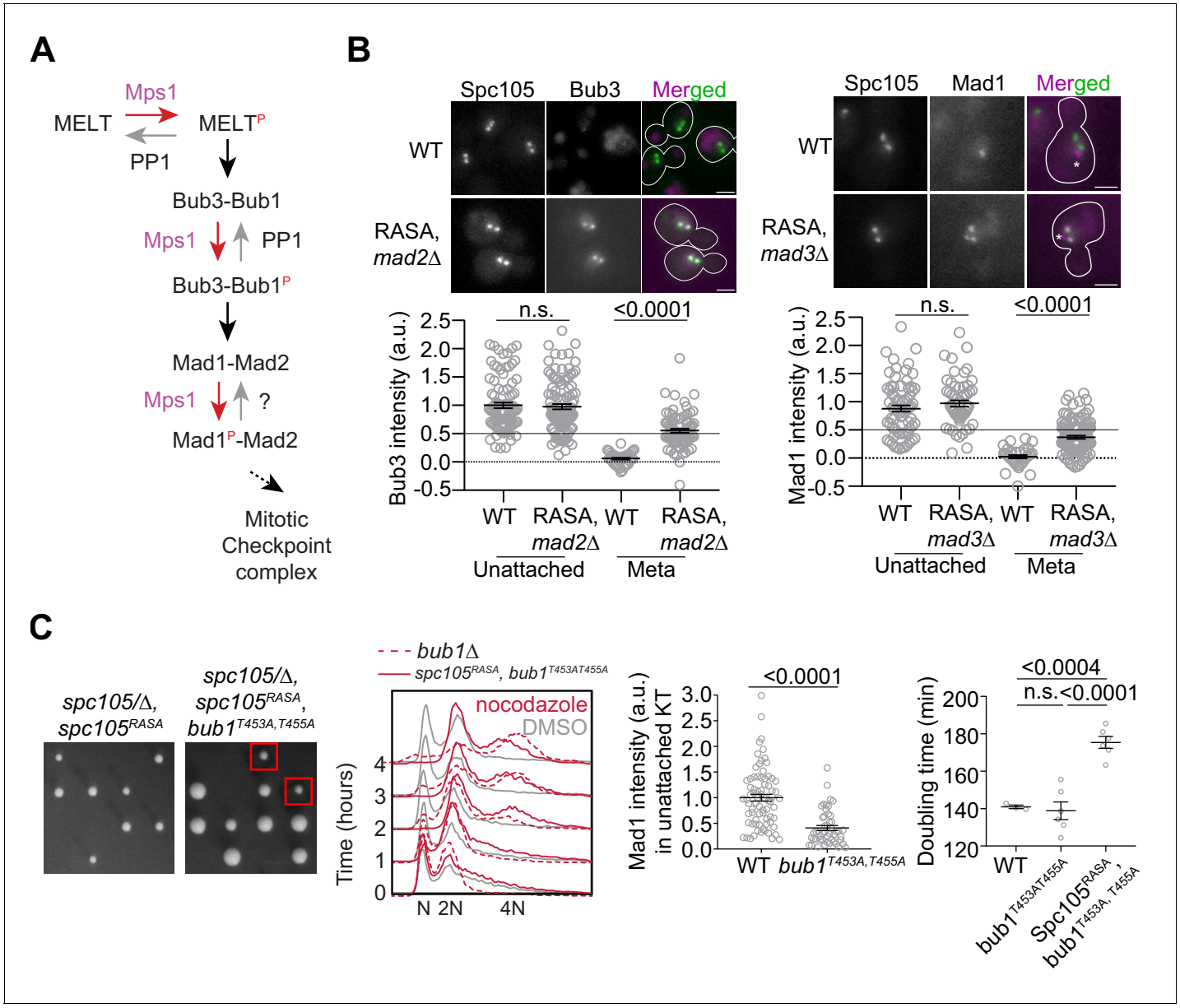

Figure 4. Revealing the determinants of the responsiveness of the SAC to PP1-mediated silencing. (**A**) A schematic of the SAC signaling cascade highlighting the potential steps that can be disrupted by Protein Phosphatase I (PP1). (**B**) Top: Representative micrographs of cells with bioriented kinetochore clusters showing the colocalization of the indicated proteins with fluorescently labeled kinetochores. Note that the Mad1-mCherry puncta marked with an asterisk result from the deletion of the nuclear pore protein Nup60. These puncta are not associated with kinetochores. The ones co-localized with kinetochores are marked with arrowheads. Scale bar ~3.2 µm. Scatter plots at the bottom show the quantification of fluorescence signal of kinetochore colocalized Bub3-mCherry and Mad1-mCherry (mean+ s.e.m., normalized to the respective average signal measured in nocodazole-treated cells). Bub3-mCherry: n = 93 and 37 for WT, 107 and 77 for Spc105^{RASA}, *mad2*Δ. Mad1-mCherry: n = 74 and 34 for WT, 60 and 111 for Spc105^{RASA}, *mad3*Δ, pooled from two technical repeats. n.s. Not significant. (**C**) Left: Tetrad dissection analysis of the indicated strains. Second from the left: Flow cytometry of DNA content of the indicated strains during prolonged exposure to nocodazole. The best of the two technical repeats is shown here. Second from the right: quantitative comparison of Mad1-mCherry recruited by unattached kinetochores in nocodazole-treated cells. (mean+ s.e.m. n = 74 for WT and 49 for *bub1*$^{453A,\ 455A}$, pooled from two experimental repeats). Right: Doubling time of the indicated strains in rich media (horizontal line indicates the mean value, obtained from at least three experimental repeats). n.s. Not significant.
The online version of this article includes the following source data for figure 4:

Source data 1. Data needed to prepare the graphs shown in ***Figure 4B*** bottom left and bottom right, 4C 2nd from the right and 4C right.

plot, second from the right). The *spc105*^{RASA} *bub1*$^{453A,\ 455A}$ double mutant exhibited a longer doubling time in YPD, which is suggestive of a SAC silencing defect arising from the lack of PP1 recruitment by Spc105 (***Figure 4C***, scatter plot on the right). Thus, PP1-mediated dephosphorylation of several phosphorylated residues on Bub1 suppresses Mad1 recruitment and thereby contributes to the responsiveness of the SAC to silencing.

These experiments clarify the distinct roles of the reduced Mps1 activity and PP1 and their effectiveness in SAC silencing. The attachment-mediated separation of the Spc105 phosphodomain and Ndc80 CH-domains along with partial dissociation of Mps1 from the CH-domains significantly reduces Mps1 kinase activity in the inner kinetochore, and makes the SAC signaling cascade responsive to PP1-mediated dephosphorylation. PP1 is then able to dephosphorylate MELT motifs and Bub1 to silence the SAC. Therefore, the efficiency of SAC silencing likely depends on the effectiveness of PP1-mediated dephosphorylation of the MELT motifs versus Bub1. PP1 must dephosphorylate multiple sites in Bub1 to completely inhibit Mad1 recruitment, whereas the dephosphorylation of just one residue in the MELT motif prevents the recruitment of both Bub3-Bub1 and Mad1. This implies that the responsiveness of SAC silencing will be determined by the PP1-mediated dephosphorylation of MELT motifs rather than Bub1. Therefore, if Bub3-Bub1-binding to the MELT motif itself interferes with MELT motif dephosphorylation, then the affinity of each MELT motif for Bub3-Bub1, and hence its sequence, will strongly influence the efficiency of its dephosphorylation.

The number of high affinity MELT motifs in Spc105 and Bub1 expression together determine SAC responsiveness to PP1-mediated silencing

To reveal the influence of the affinity of MELT motifs on SAC responsiveness to PP1-mediated silencing, we created a hyper-active Spc105 variant that we denote as #1^{6}. In this mutant, a span of 10 amino acids centered on the last five MELT motifs was replaced with the same span centered on the optimal sequence of the first MELT motif. In a large fraction of cells expressing #1^{6}, Bub1-mCherry abnormally colocalized with bioriented kinetochore clusters indicating a defect in SAC silencing (***Figure 5A***, left and ***Figure 5—figure supplement 1A***). Accordingly, the doubling time for these strains was ~14% higher compared to wild-type cells (164 vs 144 min.; ***Figure 5A***, middle scatter plot). The increased doubling time is due to the SAC, because the deletion of *MAD1* eliminated it (5A, second from the right). However, the stronger SAC activity of #1^{6} did not confer any detectable advantage to yeast cells: in media containing benomyl the growth rate and maximal cell density reached was similar for both wild-type and #1^{6} strains (***Figure 5A*** right). Therefore, the retardation of the cell cycle due to the hyper-active Spc105 allele is a fitness cost for this yeast strain, and too many high affinity MELT motifs per Spc105 are likely to be counterproductive.

The abundance of Bub3-Bub1 is also likely to influence SAC responsiveness to silencing, because in nocodazole-treated cells, only 20% of MELT motifs in unattached kinetochores recruit Bub3-Bub1, and Bub1 overexpression is sufficient to saturate these MELT motifs (***Aravamudhan et al., 2016***). To test this, we over-expressed Bub1-mCherry using the galactose-inducible *GAL1* promoter, and quantified the growth rate of cells expressing either wild-type Spc105 or #1^{6} (***Janke et al., 2004***). Upon partial induction of the *GAL1* promoter using a low galactose concentration (0.5%, that is moderate Bub1 over-expression), kinetochores retained Bub1 even after biorientation in both strains (micrographs in ***Figure 5B***, left). The doubling time of cell cultures of both strains was significantly higher, but the effect was more severe for the #1^{6} culture (***Figure 5B***, ; ***Figure 5—figure supplement 1A*** left). Upon full induction of the *GAL1* promoter activity using 2% Galactose, the growth of both strains was significantly hampered (***Figure 5—figure supplement 1B*** right and 5B). Importantly, the fold-increase in the doubling time was higher for the #1^{6} cultures compared to wild-type cell cultures in both experiments (~15% for wild-type Spc105 with either partial or full induction of the *GAL1* promoter, 35% and 66% for #1^{6} in partial and full induction conditions respectively).

These experiment along with our prior observations showing that Bub1 abundance primarily limits Mad1 recruitment to the cell show that the low expression level of Bub1 limits the recruitment of Bub3-Bub1 and Mad1-Mad2 to unattached yeast kinetochores and thus primarily limits SAC strength. The number and affinity of MELT motifs determines both the strength and the responsiveness of the SAC to PP1-mediated silencing.

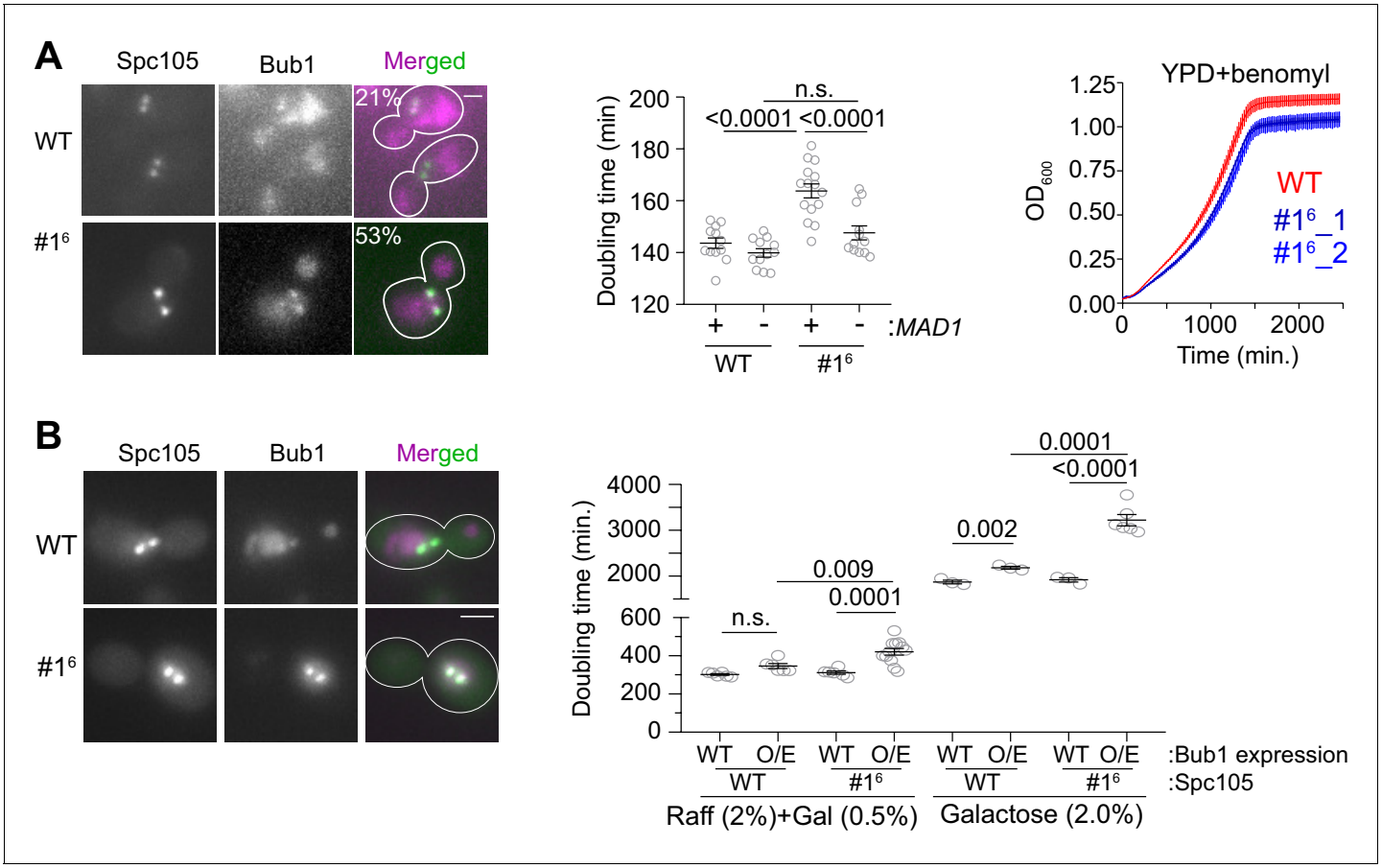

Figure 5. The influence of MELT motif activity and Bub1 expression level on the strength and responsiveness of the SAC. (**A**) Left: Representative micrographs show the recruitment of Bub1-mCherry to bioriented kinetochore clusters (%age noted at the top of each micrograph indicates the fraction of cells with Bub1-mCherry visibly recruited to bioriented kinetochore clusters; also see ***Figure 5—figure supplement 1A***) Scale bar ~3.2 µm. Second from the left: Quantification of the growth rate of indicated strains in non-selective media. Second from the right: The scatter plot shows the indicated strains (mean+ s.e.m from at least six repeats). Right: Quantification of the growth rate of indicated strains in benomyl-containing media (20 µg/ml) (mean+/-s.e.m. from n = 3). n.s. Not significant. (**B**) Left: Representative images show Bub1 recruitment at the bi-oriented kinetochores when Bub1 is overexpressed in indicated strains (n = 2). Scale bar ~3.2 µm. Right: Scatter plot shows the doubling time of the indicated strains, grown in raffinose (2%)+galactose (0.5%) and in galactose (2%). mean+ s.e.m obtained from at least six repeats. Note that the growth rates of all strains are greatly reduced, when raffinose or galactose rather glucose are used as the carbon source. n.s. Not significant.

The online version of this article includes the following source data and figure supplement(s) for figure 5:

Source data 1. The data required for creating the graphs in ***Figure 5A*** middle and right and 5B right.

Figure supplement 1. The influence of the affinity of MELT motifs to Bub3-Bub1 expression on the responsiveness of the SAC to silencing mechanisms.

Figure supplement 1—source data 1. Data needed to prepare the graphs shown in ***Figure 5—figure supplement 1A*** left and right, B left and right, D, E and F.

Engineering an Spc105 allele for optimal SAC signaling, silencing, and error correction

These findings point to a trade-off between implementing a strong SAC and one that is responsive. For a strong SAC, many high affinity MELT motifs are desirable. However, to make the SAC responsive, they must be efficiently dephosphorylated, and this requires the recruitment of PP1 via the RVSF motif in Spc105. The Spc105-PP1 interaction comes with its own cost: the PP1 recruited for SAC silencing can inadvertently stabilize syntelic attachments and thus lead to chromosome missegregation (***Roy et al., 2019***). The weakening or even complete inactivation of the Spc105-PP1 interaction leads to significantly improved chromosome segregation when chromosome biorientation is challenged (***Roy et al., 2019***). These observations suggested to us a blueprint for designing an

'optimal' Spc105 variant that: (1) avoids the harmful crosstalk between SAC silencing and chromosome biorientation due to the Spc105-PP1 interaction, (2) allows rapid SAC silencing upon chromosome biorientation, and (3) still maintains a strong SAC. To engineer this optimal variant, we anticipated that: (a) the RVSF motif must be weakened or inactivated, (b) MELT motifs must have a weak affinity for Bub3-Bub1, and (c) there should be many such MELT motifs per Spc105.

To test our hypothesis, we created two Spc105 mutants that both contain a non-functional RVSF motif (*spc105^{RASA}*) and either only the first three, strong MELT motifs (designated as #1–3) or only the last three weak ones (designated as #4–6, see **Figure 2**). Tetrad dissection analysis of the two diploid strains: *SPC105/spc105Δ leu2/leu2::spc105$^{RASA,\#1-3}$* and *SPC105/spc105Δ leu2/leu2::spc105$^{RASA,\#4-6}$* revealed that only the weaker MELT motifs suppressed the lethality caused by the non-functional RVSF motif (**Figure 6A**, also see **Figure 5—figure supplement 1C**). Thus, diffusive interactions between PP1 and Spc105 appear to be sufficient to dephosphorylate the weak MELT motifs, but not for the strong motifs. The simplest explanation this observation is that Bub3-Bub1 binding to the MELT motif hampers the ability of PP1 to dephosphorylate the MELT motif.

Using fluorescence microscopy, we confirmed that kinetochores in the *spc105$^{\#4-6}$* strain did not recruit Bub3-mCherry in metaphase, but recruited both Bub3 and Mad1 when unattached upon nocodazole treatment (**Figure 6B**, also see **Figure 5—figure supplement 1D** and **Figure 5—figure supplement 1E**). As expected, the SAC was sufficient to maintain 2N ploidy during prolonged nocodazole treatment (**Figure 6B**). In benomyl-containing media, this strain grew significantly faster even compared to the wild-type strain, suggesting that chromosome biorientation and chromosome segregation accuracy in this strain was improved (6C). Colony sectoring assay revealed that even under normal growth conditions, the chromosome segregation accuracy in this strain was significantly higher than the strain expressing *spc105$^{\#4-6}$* and even wild-type cells (only three red colonies out of ~6600 compared to 18 red colonies out of ~5100 for the wild-type strain, **Figure 6E**). However, the doubling time for this mutant under normal conditions was 20% higher than wild-type cells, (**Figure 6D** and **Figure 5—figure supplement 1F**). The higher doubling time is likely due to an SAC silencing defect, although this needs to be confirmed experimentally. Importantly, the slower growth rate was accompanied by improved chromosome segregation. These observations demonstrate that the balance of SAC signaling strength and its responsiveness to silencing mechanisms determines the trade-off between accurate chromosome segregation and timely anaphase onset.

PP1-mediated dephosphorylation of Bub1 prevents the tethered Spc105 phosphodomain from activating the SAC from inner kinetochore

Construction of the *spc105$^{RASA,\#4-6}$* strain also afforded us the opportunity to determine why the SAC is not activated by the Spc105 phosphodomain tethered in the inner kinetochore, even though it recruits Bub3-Bub1 robustly (**Figure 3**). We reasoned that the PP1 recruited by Spc105 dephosphorylates Bub1 bound to the tethered phosphodomain preventing it from recruiting Mad1 and thus ensuring that the SAC remains inactive (cartoon in **Figure 6F**, top). To confirm this, we tethered the Spc105 phosphodomain to Ndc80-Fkbp12 in *spc105$^{RASA,\ \#4-6}$* cells by adding rapamycin to growth media, reasoning that the Bub1 recruited by the tethered phosphodomain would now remain phosphorylated in the absence of PP1 and thus recruit Mad1. Consistent with this expectation, we found that the phosphodomain tethered at Ndc80-C robustly recruited Mad1 in cells expressing *spc105$^{RASA,\ \#4-6}$* but not wild-type Spc105 (**Figure 6F**, representative images at the middle, bar graph at the bottom left). We even observed a small number of cells with wherein Mad1 localized at the kinetochores even in anaphase (**Figure 5—figure supplement 1G**). The growth rate of cells expressing the *spc105$^{RASA,\ \#4-6}$*, but not wild-type Spc105 in media containing rapamycin was also reduced, revealing incomplete SAC silencing (6F, bottom right). These experiments demonstrate that the reduction of Mps1 kinase activity in the kinetochore primes the SAC for silencing, enabling PP1 to disrupt SAC protein recruitment.

Discussion

This study provides three critical insights into the physiological operation of the SAC signaling cascade. First, we find that the reduced SAC strength due to Spc105 mutants containing fewer or only the weak MELT motifs is apparent only in normally growing cells or when the process of

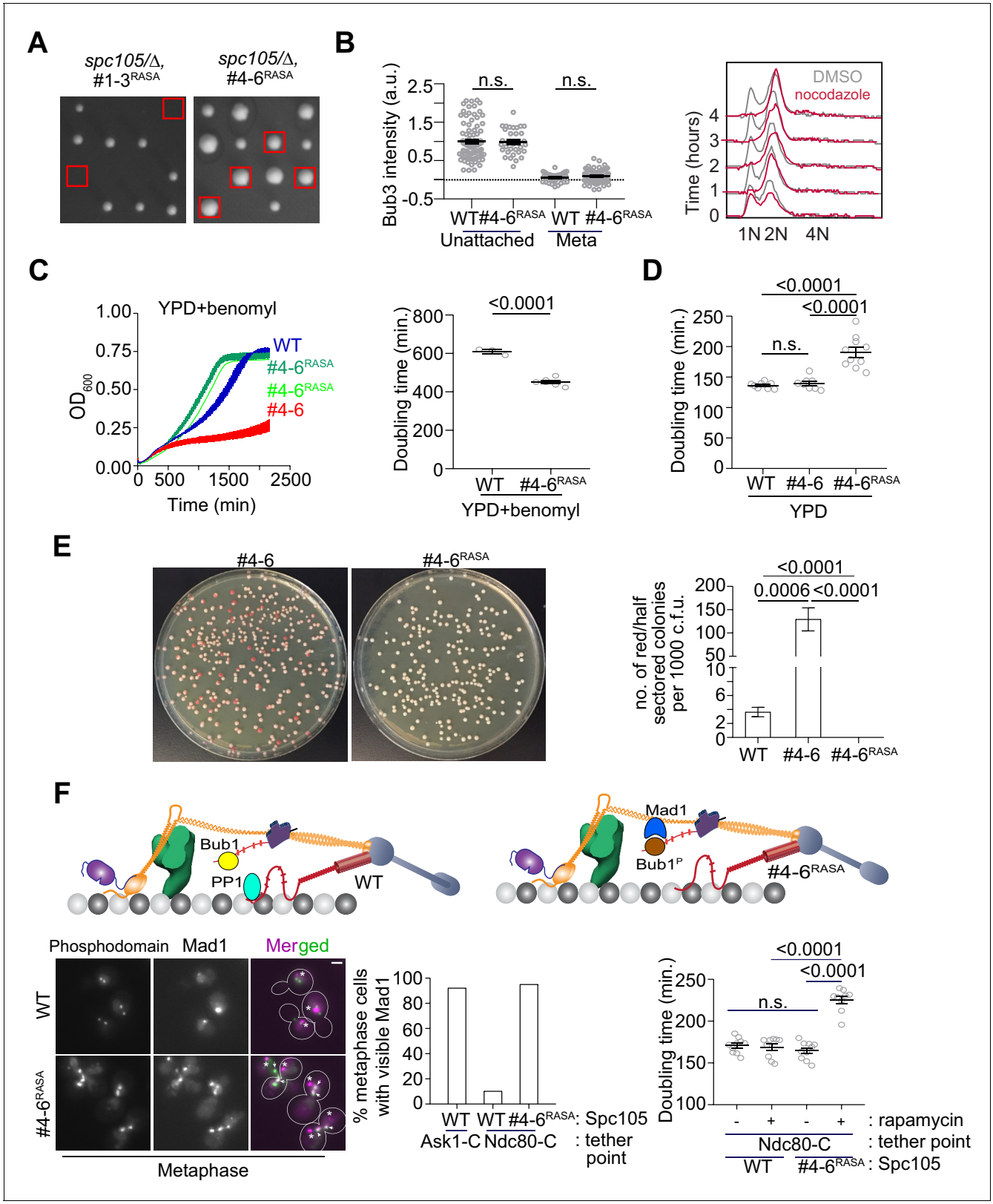

Figure 6. Designing an Spc105 variant optimized for SAC signaling, error correction, and SAC silencing. (**A**) Left: Tetrad dissections showing the rescue of Spc105^{RASA} by inactivating the first three MELT repeats. Right: Scatter plot depicting Bub3 intensities in unattached and bioriented kinetochores of indicated strains (mean+ s.e.m. n = 92 and 37 for WT, 33 and 98 for #4-6^{RASA}, pooled from two technical repeats). n.s. Not significant. (**B**) Representative flow cytometry-based quantification of the DNA content of the indicated strains during a prolonged exposure to nocodazole (n = 2). (**C**)

Figure 6 continued on next page

Figure 6 continued

Quantification of the doubling times of the indicated strain in YPD respectively (horizontal line marks the mean value, minimum number of experimental repeats n = 2).(**D**) Left: Quantification of population growth for the indicated strains in presence of benomyl (30 µg/ml) (mean ± s.e.m., n = 3). Right: Quantification of the doubling times of the indicated strain in YPD+benomyl (30 µg/ml) respectively (horizontal line marks the mean value, minimum number of experimental repeats n = 2). (**E**) Estimation of chromosome loss by colony sectoring assay. Left: Plate images of #4–6 and #4-6^{RASA} strains grown in YPD plates. Right: Bar graph displays the number of red or half sectored colonies per 1000 colony forming units. N = 5081, 4965 and 6596 for WT, #4–6 and #4-6^{RASA} respectively, pooled from ≥6 technical repeats. (**F**) Top: Model explaining why Spc105 phosphodomain tethered in the inner kinetochore does not activate the SAC. Bottom left: Representative micrographs display Mad1-mCherry localization relative to bioriented kinetochores in the indicated strains after treatment with rapamycin. The Mad1-mCherry puncta marked with an asterisk result from the deletion of the nuclear pore protein Nup60. These puncta are not associated with kinetochores. The ones co-localized with kinetochores are marked with arrowheads. Scale bar ~3.2 µM. Bottom middle: Bar graph of the percentage of cells visibly recruiting Mad1-mCherry (n = 242, 142 and 290 for Ask1-C, Ndc80-C and Ndc80-C, #4-6^{RASA} respectively, derived from two technical repeats). Bottom right: Scatter plot presents the doubling time of the indicated strains. mean+ s.e.m from ≥three experimental repeats. n.s. Not significant.

The online version of this article includes the following source data for figure 6:

Source data 1. Data required for graphs shown in ***Figure 6B and C*** left and right, 6D, 6E, 6F bottom middle and 6F bottom right.

chromosome biorientation is challenged. It is not detected in nocodazole-treated cells containing a large and constant number of unattached chromosomes. The most likely explanation for this discrepancy is that the cumulative signaling output of the large and unchanging number of unattached kinetochores in nocodazole-treated cells masks the reduced signaling output of individual kinetochores. Therefore, SAC strength measured as the duration of mitotic arrest in nocodazole-treated cells is not useful in predicting the ability of the SAC to ensure genome stability. Under normal conditions, the maintenance of genomic stability in budding yeast requires a strong SAC enabled by more than one MELT motif possessing the functionally optimal amino acid sequence. This insight provides a functional explanation for the evolutionary trend of the expansion of the number of MELT motifs in Spc105 and its homologs via recurrent duplication events (***Tromer et al., 2015***).

The second insight from our study is in the form of a clarification of the distinct roles that the microtubule-mediated reduction in Mps1 activity and PP1 play in silencing the SAC. The microtubule-mediated separation and dissociation of Mps1 significantly reduces its kinase activity, especially in the inner kinetochore beyond the Dam1 complex (***Aravamudhan et al., 2015***; ***Hiruma et al., 2015***; ***Ji et al., 2015***). This primes the SAC for silencing but doesn't completely stop it. The residual Mps1 activity can drive SAC signaling at a lower level and retard mitotic progression. This is prevented by the PP1 recruited by Spc105, which dephosphorylates the MELT motifs and Bub1 to stop the recruitment of Bub1 and Mad1 to the kinetochore. Bub1 dephosphorylation contributes to SAC silencing, however, MELT motif dephosphorylation by PP1 has a stronger impact on SAC silencing, consistent with the foundational role of the MELT motifs in the SAC signaling cascade. With this insight, we demonstrate that the number and activity of MELT motifs can be suitably balanced to make the dedicated mechanism for PP1 recruitment via Spc105 non-essential. In fact, the elimination of this interaction has a significant advantage: chromosome biorientation and error correction are improved under stressed conditions. However, this comes at the cost of delayed SAC silencing under normal conditions.

The final insight from our work is that the Bub3-Bub1 binding affinity of MELT motifs is a key determinant of the responsiveness of the SAC. When the MELT motif is bound by Bub3-Bub1, steric effects are likely to interfere with its dephosphorylation. A direct test of this hypothesis is left for future studies. Nevertheless, its main predictions are supported by our data: the high affinity MELT motifs in Spc105 are more resistant to PP1-mediated dephosphorylationand they reduce the responsiveness of the SAC to silencing. It is important to note that at a minimum, the signaling output of one unattached kinetochore has to be sufficient to delay anaphase onset until stable, end-on microtubule attachment is formed. Beyond this limit, additional signaling capacity does not offer any advantage; it is likely to increase the duration of the cell cycle unnecessarily. Therefore, beyond a certain number, additional MELT motifs per Spc105 do not contribute to the strength of the SAC. Instead, they are likely to impose a fitness cost. Therefore, the number and Bub3-Bub1 binding affinity of MELT motifs must be optimized to balance SAC strength and responsiveness. We propose that the evolution of MELT motif copy number and sequence may reflect an evolutionary process that balances SAC strength and responsiveness to ensure genomic stability and timely cell division.

Materials and methods

Key resources table

Reagent type (species) or resource	Designation	Source or reference	Identifiers	Additional information
Strain, strain background (*S. cerevisiae*)	AJY#	This paper and previous literatures.	N.A.	Detailed information of strain genotypes is provided in ***Supplementary file 2***. See plasmid and strain construction below for more details.
Recombinant DNA reagents	pAJ#	This paper or obtained by requests to other labs	N.A.	Detailed information of the recombinant DNA reagents (plasmids) used in this study is provided in ***Supplementary file 3***. See plasmid and strain construction below for more details.
Chemical compound, drug	Benomyl	Millipore Sigma	45339	Both of the benomyl powders have been used in spotting and plate reader assays. Please refer to materials and methods for concentration of Benomyl. See benomyl sensitivity assay mentioned below for more details.
Chemical compound, drug	Benomyl	Millipore Sigma	381586	
Chemical compound, drug	Nocodazole	Fisher Scientific	AC358240100	Used to disrupt spindle and create unattached kinetochores. Please see below for concentration of Nocodazole.
Chemical compound, drug	Propidium Iodide (PI)	Millipore Sigma	P4864	Used in flow cytometry. Please refer to flow cytometry section below for concentration of PI,
Chemical compound, drug	Rapamycin	Fisher Scientific	NC9362949	Used in phosphodomain tethering assays. Please see flow cytometry section for concentration of Rapamycin.
Chemical compound, drug	RNase	Fisher Scientific	SIG10109169001	Used in flow cytometry. Please refer to flow cytometry section for concentration of RNase.
Software/algorithm	Graphpad Prism	Graphpad software Inc	Prism Version 8	Used for making plots and performing statistical analyses
Software/algorithm	ImageJ (Fiji)	https://imagej.net/Fiji/Downloads		Used for Spc105, phosphodomain tethering, Bub3, Bub1, Mad1 and Sgo1 intensity measurement.
Software/algorithm	Matlab	Mathworks		For colony counting, we used Colony counter
Software/algorithm	Metamorph	Molecular devices		Used for imaging involving microscopy assays. Please refer to Materials and methods for details of imaging
Software/algorithm	Adobe Illustrator	Adobe creative cloud	Version 2019	Used to assemble the data and to prepare the figures
Other	Gene and protein information resources for *S. cerevisiae*	Saccharomyces genome database (https://www.yeastgenome.org)	N.A.	Used for recombinant DNA reagents and *S. cerevisiae* strain construction.

Plasmid and strain construction

The plasmids and *S. cerevisiae* strains used in this study are listed in ***Supplementary file 2*** and ***Supplementary file 3*** respectively. Strains containing multiple genetic modifications were constructed using standard yeast genetics. Proteins tagged with GFP(S65T) and mCherry or yeast codon optimized mCherry were used to visualize kinetochores, spindle pole bodies and SAC signaling components. A 7-amino-acid peptide (sequence: 'RIPGLIN') was used as the linker between the proteins and their C-terminal tags (GFP, mCherry or 2XFKBP12). The cassettes for gene deletion, gene replacement and C- terminal tags were introduced at the endogenous locus through homologous recombination of PCR amplicons or using linearized plasmids (***Bähler et al., 1998***). We previously observed a significant strain to strain variation in the intensity of mCherry-tagged kinetochore proteins or checkpoint proteins due to inherent variability of the brightness of mCherry. Therefore, we created all Bub3-mCherry and Mad1-mCherry strains by crossing the same transformant of either Bub3-mCherry (AJY3844 or AJY3846) or Mad1-mCherry (AJY1836 or AJY3741) with other strains. For the same reason, we created all the strains used in Forster Resonance Energy Transfer (FRET) quantification by crossing a specific transformant of Spc25-mCherry (AJY778) or Dad4-mCherry (AJY906). The deletion mutant of *NUP60* always accompanies Mad1-mCherry to disrupt Mad1localization to the nuclear envelopes (***Scott et al., 2005***). This facilitated clearer visualization and quantification of Mad1 localized to unattached kinetochores without affecting SAC strength.

To construct diploid strains, we mixed overnight grown cultures of two strains of A and α mating types and spotted the cell suspension on a YPD plate, and then incubated the cells for approximately 3–4 hr at 32˚C. To induce meiosis, we transferred stationary phase diploid cells to starvation media (yeast extract 0.1%, Potassium acetate 1%), and we incubated them at RT for 4–5 days to induce meiosis.

All the Spc105 mutants used in the study are chimeras of Spc105 and either GFP or codon optimized mCherry. Genes encoding the chimeric proteins were introduced using a cassette that consists of the 397 bp upstream and 250 bp downstream sequences of the SPC105 open reading frame as promoter (*prSPC105*) and terminator (*trSPC105*) sequences respectively. We introduced genes encoding either GFP (S65T) or a codon optimized mCherry at the 222nd, 455th, and 709th amino acid position of Spc105 by sub-cloning where we introduced an extra *Bam*HI site (Gly-Ser) at the upstream and *Nhe*I site (Ala-Ser) at the downstream of the GFP fragment. The plasmids based on pRS305 or pRS306 backbone were linearized by *Bst*EII or *Stu*I before transformations to ensure their integration at the *LEU2* or the *URA3* locus respectively.

We constructed the MELT motif mutants of Spc105 using the QuickChange II XL Site-Directed mutagenesis kit (Agilent Technologies). To build pAJ737 (Spc105_#4–6 in #1–3), we cloned a 306 bp fragment which codes for Spc105$^{223\text{-}324}$ within *Bam*HI-*Bsi*WI sites of pAJ613 (Spc105$^{\#1\text{-}3}$). To generate pAJ747 (Spc105$^{\#1\text{-}3\ in\ \#4\text{-}6}$), we used pAJ609 (Spc105_#4–6) as vector where we cloned a 274 bp fragment within *Nhe*I-*Mlu*I, that codes for Spc105$^{132\text{-}222}$. While constructing the chimeras for #2^{MELT} (pAJ867), #4^{MELT} (pAJ868) and #5^{MELT} (pAJ870), we introduced mutations of M171L, ID232-233ME and I283L respectively, but kept the flanking sequences unchanged. To design a plasmid that codes for Spc105_#1^{6} (pAJ904), we used pAJ419 (Spc105$^{455::GFP}$) as the parent vector. We used *Bsi*WI-*Bam*HI sites in that plasmid to replace the WT sequence which contains 6 MELT repeats with a 981 bp fragment which harbors 6 repeats of MELT1 and its flanking sequences (codes for PDTSGMELTE PIVATP).

To construct pAJ852 or pAJ896, which express *bub1*$^{T453A,\ T455A}$, we used the pSK954 plasmid backbone (***Kemmler et al., 2009***). pSK954 consists of the *ADH1* transcription terminator cloned within *Asc*I-*Bgl*II. We cloned the 500 bp upstream sequence that harbors *BUB1* promoter, 3.063 kb *BUB1* ORF sequence and 651 bp *2XFKBP12* within *Sac*II-*Asc*I site of this plasmid. The ORF and *2XFKBP12* are separated by 21 bp linker which codes for RIPGILK. We also cloned 350 bp downstream sequence of *BUB1* which consists of *BUB1* terminator within *Pme*I-*Apa*I. To build the strains with *bub1*$^{T453A,\ T455A}$ allele, we first created a diploid strain where one copy of *BUB1* was deleted with *TRP1*. The plasmids of pAJ852 or pAJ896 were digested by *Apa*I and SacI to release 6.279 kb fragment which recombined at the deleted bub1 locus replacing the *TRP1* cassette. There is mutation of SR (449-450)TG in *BUB1* ORF of pAJ852. However, upon testing there were no discernable phenotypic differences between the strains constructed by pAJ852 and pAJ896.

We obtained pAJ669 (BZ427) from Prof. Storchova's lab (**Peplowska et al., 2014**), which we digested by *Stu*I and transformed in yeast to obtain strains required for CIK1-CC overexpression.

Cell culture

Yeast strains were grown in YPD (yeast extract 1%, peptone 2%, dextrose 2%) or YPRG (yeast extract 1%, peptone 2%, Raffinose 2%, Galactose 0.5%) at 32˚C. Strains that express *CDC20* from *MET3* promoter were grown in synthetic dextrose media lacking methionine were used.

For the spotting assays involving CIK1-CC overexpression, we grew all the strains to mid-log phase in YPR media (yeast extract 1%, peptone 2%, Raffinose 2%). Then starting from 0.2 OD_{600} cells, we prepared serial dilutions (1:2 or 1:10) which were then spotted on either YPD or YPG agar media. All spotting assays were performed with at least two biological replicates whenever possible and two technical replicates on both YPD and YPG plates. For time course imaging experiments involving CIK1-CC overexpression, we started from overnight inoculums grown in YPR, shifted the cells to YPG media for 1.5 hr, and then supplemented the media with α factor (2 µg/ml) to arrest the cells at G1 for 2 hr. After this, we washed the cells to remove the α factor and released them in fresh YPG media. We took aliquots of cells to image and analyze 75, 105 and 135mins after the wash. For chromosome loss assay, the strains containing the nonessential linear chromosome fragment (CFIII, which contains *SUP11*) were grown in synthetic media devoid of uracil until they were diluted for plating.

Benomyl sensitivity assay

The assay was done as described previously (**Roy et al., 2019**). We used plates with both 20 µg/ml and 30 µg/ml benomyl concentration. At least two biological replicates wherever possible and two technical replicates were conducted in all the experiments. We included a wild-type positive control which grows on benomyl, and an appropriate negative control strain which either grows poorly or not at all under the same condition. We prepared benomyl supplemented YPD as it was described previously (**Gupta et al., 2018**). To track biorientation and spindle formation in benomyl-containing media, we arrested cells in G1 by exposing mid-log phase cultures to α factor (2 µg/ml) for 1 hr 45 min. G1 synchronized cells were then washed to remove the α factor, and transferred to media containing benomyl. Aliquots of these cultures drawn at 45, 75, and 105 min post-wash were used for imaging. At least 20 microscope fields were captured at each time point for analysis.

96-well plate liquid culture assay

This assay was conducted as described previously (**Hung et al., 2018**). Briefly, we initiated cultures at 0.05 OD_{600} in each well by appropriately diluting mid-log phase cultures maintaining ~160 µl final volume. For assay involving benomyl treatment, cells from mid-log phase cultures were pelleted, resuspended and diluted in YPD+benomyl liquid. For each strain, we set at least three three technical repeats in YPD or YPD+benomyl. In assays that involve rapamycin treatment, we grew the strains to mid log phase in non-selective media, and then diluted these cultures appropriately so as to initiate 0.05 OD_{600} cultures in each well grow in either YPD or YPD+rapamycin (1 µg/ml). To measure OD_{600} continuously, we placed the 96 well plate in a Spectra Max 340PC plate reader and incubated it for either 24 hr (YPD) or 36 hr (YPD+benomyl) at 30˚C without shaking. The reader measured the absorbance every 20mins. For cells growing in YPRG or YPG, we set at least three technical replicates and ran the assay for 48 hr at 30˚C without shaking. It should be noted that the growth rate of these static cultures in a 96 well plate is significantly slower than that of the same cultures grown in a flask, incubated in 30˚C shaker incubator.

Microscopy and image analysis

A Nikon Ti-E inverted microscope with a 1.4 NA, 100X, oil-immersion objective was used for all the experiments. The 1.5X opto-var lens to measure Bub1, Bub3 and Mad1-mCherry intensities. The cells were imaged at room temperature in synthetic dextrose (or synthetic galactose media whenever it was required for the assay) supplemented with essential amino acids to obtain at least 20 microscopic fields at a given time points for any strains. We added nocodazole or methionine to the mounting media to image the nocodazole arrested cells or Cdc20 depleted cells respectively. For

each field of view, a ten-plane Z-stack was acquired (200 nm separation between adjacent planes), and at least 20 fields were acquired in each experiment.

Total fluorescence intensities of kinetochore clusters (16 kinetochores in metaphase) was measured by integrating the intensities over a 6 × 6 region centered on the maximum intensity pixel. We utilized the median intensity of pixels immediately surrounding or a nearby 6 × 6 area to correct for background fluorescence. Fluorescence intensity and FRET quantification was performed as described previously (**Joglekar et al., 2006**; **Aravamudhan et al., 2014**; **Joglekar et al., 2013**).

Chromosome loss quantification

We performed the colony sectoring assay as described previously (**Duffy and Hieter, 2018**; **Warren et al., 2002**). We grew strains harboring the nonessential linear chromosome fragment (CFIII, which contains *SUP11*) to mid-log phase on selective media (synthetic media devoid of Uracil), and then plated ~200–300 cells per plate on non-selective media (YPD). The low adenine concentration in YPD aids the development of red pigments only in cells that lose the CFIII fragment; cells that propagate CFIII remain white in color. We incubated the plates at 30˚C for 3 days followed by incubation at 4˚C for 24 hr which augment the accumulation of the red pigments. To quantify the chromosome loss rate accurately, only those colonies that are either completely red or at least half red/half-sectored, that is one half of the colony is red while the other half is white, are counted, because they reflect a chromosome missegregation event in the first cell division immediately after plating. However, because the artificial chromosome is lost only 1 in 10,000 cell divisions (**Duffy and Hieter, 2018**), a very large number of cells must be plated. We expected our strain expressing the engineered *SPC105* allele to have an even smaller chromosome loss rate than wild-type strains. Therefore, we counted colonies that are either fully red or half-sectored. A fraction of the red colonies represents cells that had already lost the chromosome during the 2–3 cell divisions that occurred during growth to mid-log phase in media selecting for the CFIII fragment. Therefore, the chromosome loss rate reported in this study is expected to be significantly higher than the true chromosome loss rate of the wild type cells that maintain CFIII fragment.

Plate images were acquired using an iPhone six camera (Model # MG632LL/A, https://support.apple.com/kb/SP705?locale=en_US). The total number of colonies and the number of red colonies were counted using a custom application (app) written in Matlab. In this app, the total number of colonies on a plate was determined by intensity-based thresholding (after median and top-hat filtering to remove background variation) followed by feature segmentation using the Watershed algorithm to separate overlapping colonies or colonies that touch one another. To count the number of red colonies, the plate image was first transformed to the L*a*b color space and then thresholded along the red-green color axis. The code for this app is mentioned in Source code one and Source code 2.

Statistical analysis

Biological replicates are defined as multiple transformants or segregants of the same genotype. Technical replicates reflect the number of times each experiment was performed. The number of cells analyzed for each strain and number of experimental replications is noted in the figure legends. All statistical analysis was conducted using Graphpad Prism (version 8). To prepare the scatter plots of Bub1, Bub3 or Mad1 intensities, we normalized the data with the mean intensities obtained for wild-type controls in each experiment. We imaged each strain at least twice to obtain significant number of metaphase cells (>50) to quantify the frequency of metaphase cells with visibly recruited SAC proteins (Bub1, Bub3, or Mad1) at the kinetochores in a cell population. We scored the metaphase cell population to divide it into two groups: cells with visible SAC protein localization to bioriented kinetochores and cells without such detectable localization. We did not notice significant variation in the fraction of metaphase cells of a specific strain with visible SAC protein localization from individual experiments. Therefore, we pooled observations from all the experiments. To compare the fraction of cells with visible SAC protein localization, we applied Fisher's exact test in Graphpad Prism (version 8). To compare sample means in all other cases, we applied either the t-test or two-way ANOVA test to ascertain the statistical significance of the rest of the data using Graphpad Prism (version 8). The p-values obtained from these tests are indicated in the figures. We performed linear regression on the linear section of each growth curve (defined manually by

selecting the same OD range for all samples from each experiment). The slope of the linear section was used to calculate the doubling time as: Doubling time = [$Log_{10}(2)$]/slope.

Flow cytometry

For these experiments, we started from overnight inoculum the designated strains to obtain mid log phase cultures. We added Nocodazole to the media (final concentration 15 µg/ml) to depolymerize the spindle and activate the SAC) and rapamycin (1 µg/ml) to induce the dimerization of FRB and FKBP fused proteins (***Gillett et al., 2004***). We collected samples containing approximately 0.1 OD_{600} cells at 0, 1, 2 and 3 hr post drug addition, fixed the cells using 70% ethanol, and stored them in 4˚C overnight. Next day, we washed out the ethanol, and treated the samples with bovine pancreatic RNase (Millipore Sigma, final concentration 170 ng/µl) at 37˚C for at least 6 hr in RNase buffer (10 mM Tris pH8.0, 15 mM NaCl). Then we removed the RNase and resuspended the cells in phosphate buffered saline (PBS) and stored them in 4˚C. These samples were incubated in Propidium Iodide (Millipore Sigma, final concentration 5 µg/ml in PBS) for 1 hr at RT on the day of the assay. The stained cells were then analyzed using the LSRFortessa (BD Biosciences) in Biomedical research core facility, University of Michigan medical school. We repeated flow cytometry for each strain at least twice. The data were analyzed using the FlowJO software.

Acknowledgements

This work was funded by the 5R35-GM126983 from NIGMS. We thank Prof. Zuzana Storchova (Technical University Kaiserslautern, Germany) for sharing reagents and Prof. Mara Duncan and her lab (Department of Cell and Developmental Biology, University of Michigan Medical School) for help with the plate reader assay. We also thank Iain Cheeseman, Mara Duncan, and Yukiko Yamashita for providing feedback on this study and the manuscript.

Additional information

Funding

Funder	Grant reference number	Author
National Institutes of Health	5R35-GM126983	Ajit P Joglekar

The funders had no role in study design, data collection and interpretation, or the decision to submit the work for publication.

Author contributions

Babhrubahan Roy, Conceptualization, Data curation, Formal analysis; Simon JY Han, Data curation, Formal analysis, Methodology; Adrienne Nicole Fontan, Data curation, Formal analysis; Ajit P Joglekar, Conceptualization, Software, Funding acquisition, Methodology, Writing - original draft, Writing - review and editing

Author ORCIDs

Babhrubahan Roy https://orcid.org/0000-0003-1815-8714
Simon JY Han https://orcid.org/0000-0001-8039-510X
Ajit P Joglekar https://orcid.org/0000-0002-0607-5332

Decision letter and Author response

Decision letter https://doi.org/10.7554/eLife.55096.sa1
Author response https://doi.org/10.7554/eLife.55096.sa2

Additional files

Supplementary files

- Supplementary file 1. Table with detailed dataset obtained from flow cytometry assay depicted in ***Figure 1D***.
- Supplementary file 2. Table with details of Saccharomyces Cerevisiae strains used in this study which includes the strain numbers, their background, details of genotype and where they have used in the study.
- Supplementary file 3. The details of recombinant DNA reagents or plasmids used in this study are tabulated in this file.
- Supplementary file 4. The source code files which were used in MATLAB to count red and white colonies in the chromosome loss assays mentioned in ***Figures 2F*** and ***6E***.
- Supplementary file 5. The source code files which were used in MATLAB to count red and white colonies in the chromosome loss assays mentioned in ***Figures 2F*** and ***6E***.
- Transparent reporting form

Data availability

We have included the source data for all the graphs that are included in the main as well as figure supplements.

References

Aravamudhan P, Felzer-Kim I, Gurunathan K, Joglekar AP. 2014. Assembling the protein architecture of the budding yeast kinetochore-microtubule attachment using FRET. *Current Biology* **24**:1437–1446. DOI: https://doi.org/10.1016/j.cub.2014.05.014, PMID: 24930965

Aravamudhan P, Goldfarb AA, Joglekar AP. 2015. The kinetochore encodes a mechanical switch to disrupt spindle assembly checkpoint signalling. *Nature Cell Biology* **17**:868–879. DOI: https://doi.org/10.1038/ncb3179, PMID: 26053220

Aravamudhan P, Chen R, Roy B, Sim J, Joglekar AP. 2016. Dual mechanisms regulate the recruitment of spindle assembly checkpoint proteins to the budding yeast kinetochore. *Molecular Biology of the Cell* **27**:3405–3417. DOI: https://doi.org/10.1091/mbc.e16-01-0007, PMID: 27170178

Bähler J, Wu J-Q, Longtine MS, Shah NG, Mckenzie A, Steever AB, Wach A, Philippsen P, Pringle JR. 1998. Heterologous modules for efficient and versatile PCR-based gene targeting in *Schizosaccharomyces pombe*. *Yeast* **14**:943–951. DOI: https://doi.org/10.1002/(SICI)1097-0061(199807)14:10<943::AID-YEA292>3.0.CO;2-Y

Chen C, Whitney IP, Banerjee A, Sacristan C, Sekhri P, Kern DM, Fontan A, Kops G, Tyson JJ, Cheeseman IM, Joglekar AP. 2019. Ectopic activation of the spindle assembly checkpoint signaling cascade reveals its biochemical design. *Current Biology* **29**:104–119. DOI: https://doi.org/10.1016/j.cub.2018.11.054, PMID: 30595520

Duffy S, Hieter P. 2018. The chromosome transmission fidelity assay for measuring chromosome loss in yeast. *Methods in Molecular Biology* **1672**:11–19. DOI: https://doi.org/10.1007/978-1-4939-7306-4_2, PMID: 29043613

Faesen AC, Thanasoula M, Maffini S, Breit C, Müller F, van Gerwen S, Bange T, Musacchio A. 2017. Basis of catalytic assembly of the mitotic checkpoint complex. *Nature* **542**:498–502. DOI: https://doi.org/10.1038/nature21384, PMID: 28102834

Gillett ES, Espelin CW, Sorger PK. 2004. Spindle checkpoint proteins and chromosome-microtubule attachment in budding yeast. *Journal of Cell Biology* **164**:535–546. DOI: https://doi.org/10.1083/jcb.200308100, PMID: 14769859

Gupta A, Evans RK, Koch LB, Littleton AJ, Biggins S. 2018. Purification of kinetochores from the budding yeast *Saccharomyces cerevisiae*. *Methods in Cell Biology* **144**:349–370. DOI: https://doi.org/10.1016/bs.mcb.2018.03.023, PMID: 29804677

Hieter P, Mann C, Snyder M, Davis RW. 1985. Mitotic stability of yeast chromosomes: a colony color assay that measures nondisjunction and chromosome loss. *Cell* **40**:381–392. DOI: https://doi.org/10.1016/0092-8674(85)90152-7, PMID: 3967296

Hiruma Y, Sacristan C, Pachis ST, Adamopoulos A, Kuijt T, Ubbink M, von Castelmur E, Perrakis A, Kops GJ. 2015. CELL DIVISION CYCLE competition between MPS1 and microtubules at Kinetochores regulates spindle checkpoint signaling. *Science* **348**:1264–1267. DOI: https://doi.org/10.1126/science.aaa4055, PMID: 26068855

Hoyt MA, Totis L, Roberts BT. 1991. *S. cerevisiae* genes required for cell cycle arrest in response to loss of microtubule function. *Cell* **66**:507–517. DOI: https://doi.org/10.1016/0092-8674(81)90014-3, PMID: 1651171

Hung CW, Martínez-Márquez JY, Javed FT, Duncan MC. 2018. A simple and inexpensive quantitative technique for determining chemical sensitivity in *Saccharomyces cerevisiae*. *Scientific Reports* **8**:11919. DOI: https://doi.org/10.1038/s41598-018-30305-z, PMID: 30093662

Janke C, Magiera MM, Rathfelder N, Taxis C, Reber S, Maekawa H, Moreno-Borchart A, Doenges G, Schwob E, Schiebel E, Knop M. 2004. A versatile toolbox for PCR-based tagging of yeast genes: new fluorescent proteins, more markers and promoter substitution cassettes. *Yeast* **21**:947–962. DOI: https://doi.org/10.1002/yea.1142, PMID: 15334558

Ji Z, Gao H, Yu H. 2015. CELL DIVISION CYCLE kinetochore attachment sensed by competitive Mps1 and microtubule binding to Ndc80C. *Science* **348**:1260–1264. DOI: https://doi.org/10.1126/science.aaa4029, PMID: 26068854

Ji Z, Gao H, Jia L, Li B, Yu H. 2017. A sequential multi-target Mps1 phosphorylation cascade promotes spindle checkpoint signaling. *eLife* **6**:e22513. DOI: https://doi.org/10.7554/eLife.22513, PMID: 28072388

Jin F, Liu H, Li P, Yu HG, Wang Y. 2012. Loss of function of the Cik1/Kar3 motor complex results in chromosomes with syntelic attachment that are sensed by the tension checkpoint. *PLOS Genetics* **8**:e1002492. DOI: https://doi.org/10.1371/journal.pgen.1002492, PMID: 22319456

Joglekar AP, Bouck DC, Molk JN, Bloom KS, Salmon ED. 2006. Molecular architecture of a kinetochore-microtubule attachment site. *Nature Cell Biology* **8**:581–585. DOI: https://doi.org/10.1038/ncb1414, PMID: 16715078

Joglekar AP, Bloom K, Salmon ED. 2009. In vivo protein architecture of the eukaryotic kinetochore with nanometer scale accuracy. *Current Biology* **19**:694–699. DOI: https://doi.org/10.1016/j.cub.2009.02.056, PMID: 19345105

Joglekar A, Chen R, Lawrimore J. 2013. A sensitized emission based calibration of FRET efficiency for probing the architecture of macromolecular machines. *Cellular and Molecular Bioengineering* **6**:369–382. DOI: https://doi.org/10.1007/s12195-013-0290-y, PMID: 24319499

Kawashima SA, Yamagishi Y, Honda T, Ishiguro K, Watanabe Y. 2010. Phosphorylation of H2A by Bub1 prevents chromosomal instability through localizing shugoshin. *Science* **327**:172–177. DOI: https://doi.org/10.1126/science.1180189, PMID: 19965387

Kemmler S, Stach M, Knapp M, Ortiz J, Pfannstiel J, Ruppert T, Lechner J. 2009. Mimicking Ndc80 phosphorylation triggers spindle assembly checkpoint signalling. *The EMBO Journal* **28**:1099–1110. DOI: https://doi.org/10.1038/emboj.2009.62, PMID: 19300438

Koch LB, Opoku KN, Deng Y, Barber A, Littleton AJ, London N, Biggins S, Asbury CL. 2019. Autophosphorylation is sufficient to release Mps1 kinase from native kinetochores. *PNAS* **116**:17355–17360. DOI: https://doi.org/10.1073/pnas.1901653116, PMID: 31405987

Krenn V, Overlack K, Primorac I, van Gerwen S, Musacchio A. 2014. KI motifs of human Knl1 enhance assembly of comprehensive spindle checkpoint complexes around MELT repeats. *Current Biology* **24**:29–39. DOI: https://doi.org/10.1016/j.cub.2013.11.046, PMID: 24361068

Liu D, Vleugel M, Backer CB, Hori T, Fukagawa T, Cheeseman IM, Lampson MA. 2010. Regulated targeting of protein phosphatase 1 to the outer kinetochore by KNL1 opposes aurora B kinase. *The Journal of Cell Biology* **188**:809–820. DOI: https://doi.org/10.1083/jcb.201001006, PMID: 20231380

London N, Ceto S, Ranish JA, Biggins S. 2012. Phosphoregulation of Spc105 by Mps1 and PP1 regulates Bub1 localization to kinetochores. *Current Biology* **22**:900–906. DOI: https://doi.org/10.1016/j.cub.2012.03.052, PMID: 22521787

London N, Biggins S. 2014. Mad1 kinetochore recruitment by Mps1-mediated phosphorylation of Bub1 signals the spindle checkpoint. *Genes & Development* **28**:140–152. DOI: https://doi.org/10.1101/gad.233700.113, PMID: 24402315

Meadows JC, Shepperd LA, Vanoosthuyse V, Lancaster TC, Sochaj AM, Buttrick GJ, Hardwick KG, Millar JBA. 2011. Spindle Checkpoint silencing requires association of PP1 to both Spc7 and kinesin-8 motors. *Developmental Cell* **20**:739–750. DOI: https://doi.org/10.1016/j.devcel.2011.05.008, PMID: 21664573

Musacchio A. 2015. The molecular biology of spindle assembly checkpoint signaling dynamics. *Current Biology* **25**:R1002–R1018. DOI: https://doi.org/10.1016/j.cub.2015.08.051, PMID: 26485365

Overlack K, Primorac I, Vleugel M, Krenn V, Maffini S, Hoffmann I, Kops GJ, Musacchio A. 2015. A molecular basis for the differential roles of Bub1 and BubR1 in the spindle assembly checkpoint. *eLife* **4**:e05269. DOI: https://doi.org/10.7554/eLife.05269, PMID: 25611342

Peplowska K, Wallek AU, Storchova Z. 2014. Sgo1 regulates both condensin and Ipl1/Aurora B to promote chromosome biorientation. *PLOS Genetics* **10**:e1004411. DOI: https://doi.org/10.1371/journal.pgen.1004411, PMID: 24945276

Primorac I, Weir JR, Chiroli E, Gross F, Hoffmann I, van Gerwen S, Ciliberto A, Musacchio A. 2013. Bub3 reads phosphorylated MELT repeats to promote spindle assembly checkpoint signaling. *eLife* **2**:e01030. DOI: https://doi.org/10.7554/eLife.01030, PMID: 24066227

Qian J, García-Gimeno MA, Beullens M, Manzione MG, Van der Hoeven G, Igual JC, Heredia M, Sanz P, Gelens L, Bollen M. 2017. An Attachment-Independent biochemical timer of the spindle assembly checkpoint. *Molecular Cell* **68**::715–730. DOI: https://doi.org/10.1016/j.molcel.2017.10.011

Rosenberg JS, Cross FR, Funabiki H. 2011. KNL1/Spc105 recruits PP1 to silence the spindle assembly checkpoint. *Current Biology* **21**:942–947. DOI: https://doi.org/10.1016/j.cub.2011.04.011, PMID: 21640906

Roy B, Verma V, Sim J, Fontan A, Joglekar AP. 2019. Delineating the contribution of Spc105-bound PP1 to spindle checkpoint silencing and kinetochore microtubule attachment regulation. *Journal of Cell Biology* **218**:3926–3942. DOI: https://doi.org/10.1083/jcb.201810172, PMID: 31649151

Scott RJ, Lusk CP, Dilworth DJ, Aitchison JD, Wozniak RW. 2005. Interactions between Mad1p and the nuclear transport machinery in the yeast *Saccharomyces cerevisiae*. *Molecular Biology of the Cell* **16**:4362–4374. DOI: https://doi.org/10.1091/mbc.e05-01-0011, PMID: 16000377

Tanaka K, Mukae N, Dewar H, van Breugel M, James EK, Prescott AR, Antony C, Tanaka TU. 2005. Molecular mechanisms of kinetochore capture by spindle microtubules. *Nature* **434**:987–994. DOI: https://doi.org/10.1038/nature03483, PMID: 15846338

Tipton AR, Ji W, Sturt-Gillespie B, Bekier ME, Wang K, Taylor WR, Liu ST. 2013. Monopolar spindle 1 (MPS1) kinase promotes production of closed MAD2 (C-MAD2) conformer and assembly of the mitotic checkpoint complex. *Journal of Biological Chemistry* **288**:35149–35158. DOI: https://doi.org/10.1074/jbc.M113.522375, PMID: 24151075

Tromer E, Snel B, Kops GJ. 2015. Widespread recurrent patterns of rapid repeat evolution in the kinetochore scaffold KNL1. *Genome Biology and Evolution* **7**:2383–2393. DOI: https://doi.org/10.1093/gbe/evv140, PMID: 26254484

Vleugel M, Tromer E, Omerzu M, Groenewold V, Nijenhuis W, Snel B, Kops GJ. 2013. Arrayed BUB recruitment modules in the kinetochore scaffold KNL1 promote accurate chromosome segregation. *The Journal of Cell Biology* **203**:943–955. DOI: https://doi.org/10.1083/jcb.201307016, PMID: 24344183

Vleugel M, Omerzu M, Groenewold V, Hadders MA, Lens SMA, Kops G. 2015. Sequential multisite phospho-regulation of KNL1-BUB3 interfaces at Mitotic kinetochores. *Molecular Cell* **57**:824–835. DOI: https://doi.org/10.1016/j.molcel.2014.12.036, PMID: 25661489

Warren CD, Brady DM, Johnston RC, Hanna JS, Hardwick KG, Spencer FA. 2002. Distinct chromosome segregation roles for spindle checkpoint proteins. *Molecular Biology of the Cell* **13**:3029–3041. DOI: https://doi.org/10.1091/mbc.e02-04-0203, PMID: 12221113

Zhang G, Lischetti T, Nilsson J. 2014. A minimal number of MELT repeats supports all the functions of KNL1 in chromosome segregation. *Journal of Cell Science* **127**:871–884. DOI: https://doi.org/10.1242/jcs.139725